Inorganics **2014**, *2*, 565-590; doi:10.3390/inorganics2040565

OPEN ACCESS

inorganics

ISSN 2304-6740

www.mdpi.com/journal/inorganics

Article

Attachment of Luminescent Neutral "Pt(pq)(C≡C^{t}Bu)" Units to Di and Tri *N*-Donor Connecting Ligands: Solution Behavior and Photophysical Properties

Elena Lalinde [1,*], M. Teresa Moreno [1,*], Santiago Ruiz [1] and Sergio Sánchez [2]

[1] Departamento de Química-Centro de Síntesis Química de La Rioja, (CISQ), Universidad de La Rioja, 26006, Logroño, Spain; E-Mail: santiago.ruiz@unirioja.es

[2] School of Chemistry, University of Manchester, Oxford Road, Manchester M13 9PL, UK; E-Mail: sergio.sanchez@manchester.ac.uk

* Authors to whom correspondence should be addressed; E-Mails: elena.lalinde@unirioja.es (E.L.); teresa.moreno@unirioja.es (M.T.M.); Tel.: +34-941-299-643 (E.L.); +34-941-299-645 (M.T.M.).

External Editor: Axel Klein

Received: *16 September 2014; in revised form: 9 October 2014* / *Accepted*: *9 October 2014* / *Published*: *31 October 2014*

Abstract: Binuclear derivatives [{Pt(pq)(C≡C^{t}Bu)}$_2$(μ-L)] (**1a**–**5a**), containing a series of dinitrogen linker ligands and the trinuclear [{Pt(pq)(C≡C^{t}Bu)}$_3$(μ-L)] (**6a**) [L = μ-1,3,5-tris(pyridine-4-ylethynyl)benzene], formed by bridge-splitting reactions with [Pt(pq)(μ-κ*C*$^\alpha$:η^2-C≡C^{t}Bu)]$_2$ (**Pt-1**), are reported. The complexes are characterized by a combination of ^{1}H NMR spectroscopy, mass spectrometry and X-ray crystallography (**2a** and **4a**). ^{1}H NMR proves the existence of a dynamic equilibrium in solution between the diplatinum complexes (species **a**), the corresponding mononuclear complex with terminal *N*-donor ligands (species **b**), the starting material (**Pt-1**) and the free ligand (L). The effects of concentration, temperature and solvent properties on the equilibrium have been studied. The optical properties of these systems have been investigated by UV-visible absorption and emission spectroscopies in solid state and in solution, and the nature of the transitions and the excited state analyzed by theoretical calculations on **2a**.

Keywords: alkynyl; cyclometalated; luminescence; platinum; *N*-donor ligands

---

1. Introduction

The interest of alkynyl platinum(II) complexes stems from their rich structural diversity [1–4], their interesting chemical reactivity [1] and more recently from their increasing potential in material science [5–17]. In this field, light-emitting complexes have attracted a great deal of attention owing to their use in optoelectronic devices, chemosensors, photovoltaic cells and photocatalysis.

By using the triple bond of the alkynyl ligand, a good number of di- and triplatinum complexes in which the Pt(II) centers are stabilized by double bridging alkynyl systems with different conformations have been reported [18–29]. However, the reactivity of these systems has been scarcely explored. It has been reported that binuclear Pt derivatives such as [*trans*-Pt(μ-κC^{α}:η^2-C≡CR)(C_6F_5)L]$_2$ or cycloplatinate complexes [Pt(C^P)(μ-κC^{α}:η^2-C≡CR)]$_2$ undergo bridge-splitting with classical donor ligands to give mononuclear σ-alkynyl Pt(II) complexes [18,23,24,27].

On the other hand, since the discovery in 1990 by Fujita of the first example of a rationally designed metallacycle, the molecular square [{Pd(en)(μ-4,4'-bpy)}$_4$](NO_3)$_8$, prepared by self-assembly of [Pd(en)(ONO_2)$_2$] (en = ethylenediamine) with the linear linker 4,4'-bipyridine (4,4'-bpy) [30], there has been increasing interest in using linear, angular, triangular or flexible linkers with bidentate or tridentate binding nitrogen units to produce fascinating metal-mediated molecular architectures, including many macrocycles and cages. Several reviews have thoroughly covered this amazing field in the last years [31–39]. The inherent stability and rather low reactivity of the Pt(II) in contrast with other metals [*i.e.*, Pd(II)] [40,41] has been the main attraction for the use of Pt(II) units for metallamacrocycles [42]. Furthermore, the attractive photophysical properties of Pt(II) complexes, such as low-energy, tunability and long-lived excited states, have prompted their incorporation into metallacycles [43–47]. The combination of the luminescent Pt(II) units in the corners with luminophore *N*-groups that can act as linkers can be exploited in highly emissive metallacycles [48]. Comparatively, platinum binuclear derivatives bridged by dinitrogen donor ligands are less represented [49–56], and particularly those with cycloplatinated fragments are scarce [49–53].

In this context, we have recently reported the synthesis and photophysical properties of the series [Pt(pq)(μ-κC^{α}:η^2-C≡CR)]$_2$ (Hpq = phenylquinoline; R = ^{t}Bu, Tol, C_6H_4OMe-3, $C_6H_4CF_3$-4) [57], which represent the first examples of cyclometalated double alkynyl bridging complexes in which the photoluminescent properties have been studied. The photophysical properties are clearly influenced by the substituents on the alkynyl ligands in response to the variation of the Pt···Pt distance. Thus, whereas the *ter*-butyl derivative with a short Pt···Pt distance displays an emission originated from a mixed metal-metal-alkynyl to pq ^{3}[(MM + L')LCT] excited state, in the aryl derivatives with a longer Pt···Pt distance, the emission arises from a ^{3}L'LCT excited state with a small or negligible contribution of ^{3}MMLCT character.

In this work, we study the reactivity of the *ter*-butyl derivative [Pt(pq)(μ-κC^{α}:η^2-C≡CR)]$_2$ (**Pt-1**) towards bidentate and tridentate nitrogen linkers, assuming that both, the "Pt(pq)(C≡C^{t}Bu)" fragment and the linkers, are luminophores. This study has allowed us to synthesize a series of platinum(II) binuclear derivatives [{Pt(pq)(C≡C^{t}Bu)}$_2$(μ-L)] bridged by *N*-*N*-donor ligands [L = pyrazine (pyz) **1a**, 4,4'-bipyridine (bpy) **2a**, 1,2-bis(bipyridyl)ethane (bpa) **3a**, *trans*-1,2-bis(4-pyridyl)ethylene (bpe) **4a** and 1,2-bis(4-pyridyl)acetylene (bpac) **5a**], and the trinuclear branched derivative [{Pt(pq)(C≡C^{t}Bu)}$_3$(μ-L)] (**6a**) containing the rigid conjugated pyridyl alkynyl ligand

[μ-1,3,5-tris(pyridine-4-ylethynyl)benzene]. A combination of crystallography (**2a** and **4a**), NMR, IR and mass spectrometry provides a complete picture of the equilibrium established in solution between derivatives with *N*-donor bridging ligands (**1a**–**5a**), mononuclear complexes with terminal *N*-ligands [Pt(pq)(C≡C^{t}Bu)(L-κ*N*)] (**1b**–**5b**) and the precursor (**Pt-1**). Furthermore, we discuss the photophysical properties of these complexes in solid state and in solution and the theoretical calculations of **2a**.

2. Results and Discussion

2.1. Synthesis and Characterization

As illustrated in Scheme 1, the synthesis of the new diplatinum derivatives [{Pt(pq)(C≡C^{t}Bu)}$_2$(μ-L)] (L = pyz **1a**, bpy **2a**, bpa **3a**, bpe **4a**, bpac **5a**) was achieved by bridged-cleavage reaction in CH_2Cl_2 of [Pt(pq)(μ-κC^{α}:η^2-C≡C^{t}Bu)]$_2$ (**Pt-1**) with the corresponding dinitrogen donor ligand. Complexes **2a**, **3a** and **5a** were obtained as orange solids in moderate (**2a**) or high (**3a**, **5a**) yields by reaction of the starting material with one equivalent of the ligand, whereas for **1a** and **4a** two equivalents of ligand were added to obtain the complexes pure in solid state. A particularly reliable indicator of the final reaction is the lack of bridging *υ*(C≡C) band in the IR spectra of the final solid (see below). On the other hand, the branched trinuclear platinum complex [{Pt(pq)(C≡C^{t}Bu)}$_3$(μ-tpab)] (**6a**) was obtained using the same strategy but with a **Pt-1**:ligand molar ratio of 3:2.

Scheme 1. Synthesis of the derivatives **1a**–**6a**.

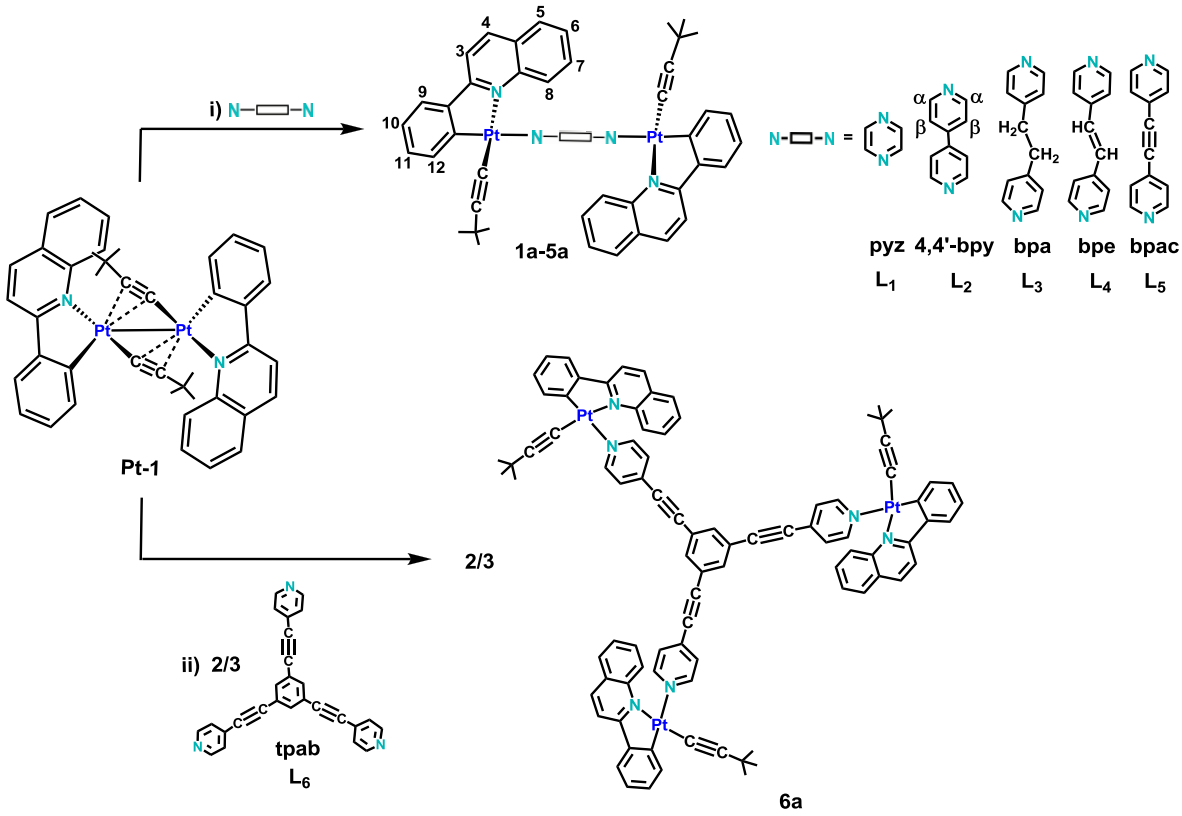

A combination of crystallography (**2a** and **4a**), IR spectra, mass spectrometry and elemental analysis supports the formulation proposed in the Scheme 1. ^{1}H NMR spectroscopy completes the

picture in solution. The IR spectra of these complexes show one υ(C≡C) intense absorption (2114–2118 cm^{-1}) in the typical range for terminal σ-coordinated alkynyl ligands, thus confirming the cleavage of the alkynyl bridging (μ-C≡C^{t}Bu)$_2$ system. Furthermore, complexes **5a** and **6a** show one additional band at higher frequency (2223 **5a**, 2212 cm^{-1} **6a**), assigned to the υ(C≡C) stretch of the inner ethynyl entity of the 4-pyridylacetylene groups in the bpac and the tpab ligands. Because of the weak coordinative bonds, ESI is used as a soft ionization method. Analysis of the complexes in CH_2Cl_2 in the positive ion mode (exact mass) gave the corresponding molecular peak for each complex and the fragmentation peak [Pt(pq)(C≡C^{t}Bu)L]$^+$ or [Pt$_2$(pq)$_2$(C≡C^{t}Bu)$_2$L]$^+$ (**6a**) by loss of the fragment [Pt(pq)(C≡C^{t}Bu)] (Figure 1). The cleavage occurs at the Pt-N covalent bond, indicating that this is the weakest link in this series of derivatives. In these complexes, there are common peaks associated with the starting material: the intact doubly σ-π alkynyl bridging molecular ion ([{Pt(pq)(C≡C^{t}Bu)}$_2$]$^+$, *m*/*z* 961), the loss of an alkynyl group ([Pt$_2$(pq)$_2$(C≡C^{t}Bu)]$^+$, *m*/*z* 879) and the cleavage ([Pt(pq)(C≡C^{t}Bu)]$^+$, *m*/*z* 481). In good qualitative agreement with the observations in the NMR spectra in solution (see below), these peaks are very intense in the mass spectra.

Figure 1. Experimental isotope pattern and predicted isotopic distribution (green) in the electrospray mass spectrum of **6a**, showing the peak [Pt$_3$(pq)$_3$(C≡C^{t}Bu)$_3$(tpab)]$^+$.

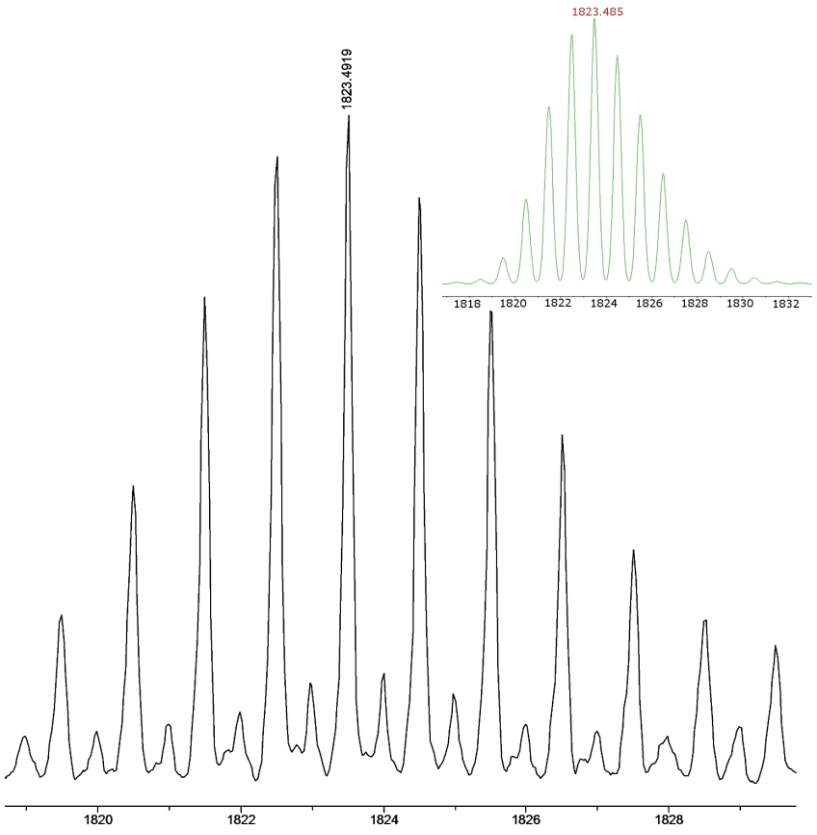

Single crystals suitable for X-ray analysis were grown by slow diffusing of *n*-hexane into a $CHCl_3$ solution at −30 °C of **2a** and **4a**, respectively. The structures of [{Pt(pq)(μ-C≡C^{t}Bu)}$_2$(μ-4,4'-bpy)]·2$CHCl_3$·C_6H_{14} (**2a**·2$CHCl_3$·C_6H_{14}) and [{Pt(pq)(μ-C≡C^{t}Bu)}$_2$(μ-bpe)]·4$CHCl_3$ (**4a**·4$CHCl_3$) were confirmed by X-ray crystallography (Figures 2, 3 and S1; Tables 1 and S1). The asymmetric unit of **2a** contains only one molecule, whereas in **4a** the asymmetric unit is formed by one independent

molecule together with two half molecules, which are completed by application of the symmetry elements. The conformation and metrical parameters of the three molecules are comparable, therefore, only the data for one of them are included in Table 1. The complexes are binuclear with a 4,4'-bpy (**2a**) or bpe (**4a**) group bridging the Pt(II) centers, which complete their distorted square planar environment with a bidentate pq ligand and one terminal alkynyl group. In both complexes, the *N*-pyridine bridging group is *trans* to the cyclometalated carbon, thus confirming that the reactions takes place with retention of the geometry in the precursor, and the Pt units adopt an *anti*-configuration.

Figure 2. View of the molecular structure of the complex [{Pt(pq)(C≡C^{t}Bu)}$_2$(μ-4,4'-bpy)]·2CHCl$_3$·C$_6$H$_{14}$ (**2a**·2CHCl$_3$·C$_6$H$_{14}$).

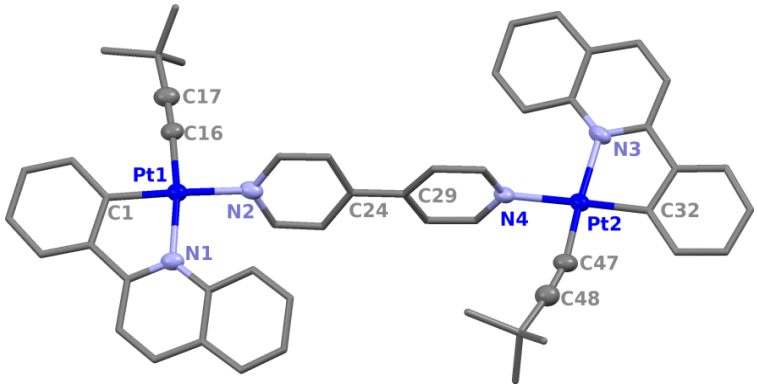

Figure 3. View of the independent molecule in the asymmetric unit in the molecular structure of the complex [{Pt(pq)(C≡C^{t}Bu)}$_2$(μ-bpe)]·4CHCl$_3$ (**4a**·4CHCl$_3$).

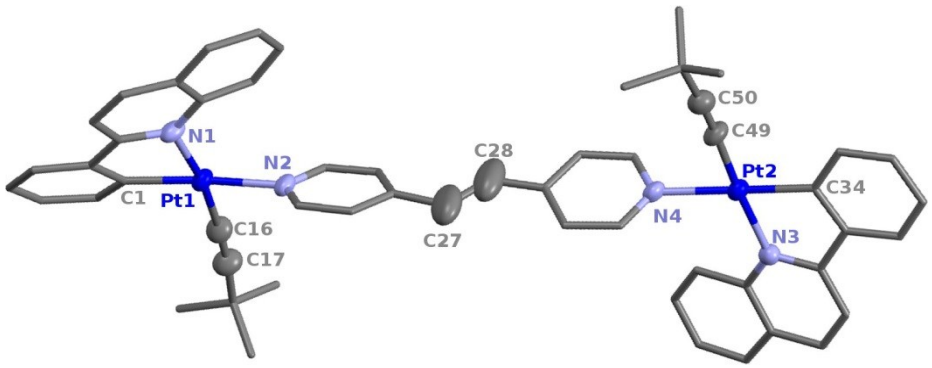

In **2a**, the two pyridyl rings form a dihedral angle between them of 16.45° (**2a**), whereas in the bpe-complex (**4a**) is of 24.0° in the complete molecule. However, due to symmetry, both rings are coplanar in the other molecules of **4a**. The bpy and bpe groups form dihedral angles with each platinum coordination plane of 67.47°, 82.18° (**2a**) and 60.36–80.41° (**4a**), respectively. These complexes show a greater variability in the angles than that observed for the related binuclear complexes with the tridentate cyclometalating pip$_2$NCN$^-$ ligand [{Pt(pip$_2$NCN)}$_2$(μ-NN)]$^{2+}$ [NN = bpy 86°, bpe 85.2°, pip$_2$NCNH = 1,3-bis(piperidylmethyl)benzene)] [49,50], but the Pt-N (bpy or bpe) distances [2.113(4), 2.125(4) Å **2a**, 2.114(7)–2.145(7) Å **4a**] are comparable. The details of the central C=C fragment in the three molecules of **4a** [range C-C 1.240(19)–1.334(17) Å] and those of the terminal alkynyl units in both complexes are not unusual (see Tables 1 and S1). The phenylquinolyl (pq) ligand is fluttered, forming dihedral angles of 13.33°, 13.97° (**2a**) and 19.82°, 9.97°, 20.02°, 10.04°

(**4a**) with the Pt coordination planes, which is consistent with other complexes containing the "Pt(pq)" metallacycle [57].

Table 1. Selected bond lengths and angles for [{Pt(pq)(C≡C^{t}Bu)}$_2$(μ-4,4'-bpy)]·2CHCl$_3$·C$_6$H$_{14}$ (**2a**·2CHCl$_3$·C$_6$H$_{14}$) and [{Pt(pq)(C≡C^{t}Bu)}$_2$(μ-bpe)]·4CHCl$_3$ (**4a**·4CHCl$_3$) (independent molecule).

2a·2CHCl$_3$·hexane		**4a**·4CHCl$_3$	
Distances (Å)			
Pt(1)-C(1)	1.994(5)	Pt(1)-C(1)	1.972(9)
Pt(1)-N(1)	2.115(4)	Pt(1)-N(1)	2.096(7)
Pt(1)-C(16)	1.967(5)	Pt(1)-C(16)	1.949(9)
Pt(1)-N(2)	2.113(4)	Pt(1)-N(2)	2.130(7)
C(16)-C(17)	1.197(7)	C(16)-C(17)	1.209(12)
Pt(2)-C(32)	1.980(5)	Pt(2)-C(34)	1.979(8)
Pt(2)-N(3)	2.127(4)	Pt(2)-N(3)	2.136(7)
Pt(2)-C(47)	1.961(5)	Pt(2)-C(49)	1.956(9)
Pt(2)-N(4)	2.125(4)	Pt(2)-N(4)	2.145(7)
C(47)-C(48)	1.209(7)	C(49)-C(50)	1.195(12)
-	-	C(27)-C(28)	1.290(9)
Angles (°)			
N(1)-Pt(1)-C(1)	80.9(2)	N(1)-Pt(1)-C(1)	80.3(3)
C(16)-Pt(1)-C(1)	91.7(2)	C(16)-Pt(1)-C(1)	92.1(4)
C(16)-Pt(1)-N(2)	88.50(19)	C(16)-Pt(1)-N(2)	87.8(3)
N(1)-Pt(1)-N(2)	98.56(16)	N(1)-Pt(1)-N(2)	99.4(3)
Pt(1)-C(16)-C(17)	175.2(5)	Pt(1)-C(16)-C(17)	176.3(9)
C(16)-C(17)-C(18)	176.6(8)	C(16)-C(17)-C(18)	175.4(11)
N(3)-Pt(2)-C(32)	80.6(2)	N(3)-Pt(2)-C(34)	80.9(3)
C(47)-Pt(2)-C(32)	95.8(2)	C(49)-Pt(2)-C(34)	93.0(4)
C(47)-Pt(2)-N(4)	81.36(19)	C(49)-Pt(2)-N(4)	83.9(3)
N(3)-Pt(2)-N(4)	101.96(16)	N(3)-Pt(2)-N(4)	102.0(3)
Pt(2)-C(47)-C(48)	167.6(5)	Pt(2)-C(49)-C(50)	174.7(9)
C(47)-C(48)-C(49)	172.7(6)	C(49)-C(50)-C(51)	174.6(11)
C(27)-C(28)-C(31)	126.5(14)	C(24)-C(27)-C(28)	121.4(14)

The crystal packing of **2a** shows that the molecules are arranged forming dimers through moderate intermolecular π···π (pq···pq) interactions (3.271, 3.336 Å, Figure S2a), which interacts through secondary interactions with the crystallization solvents ($CHCl_3$, *n*-hexane) and with other dimers ($H_{py}\cdots\pi_{C\equiv C}/C_{pq}$) (Figures S2b). However, the supramolecular structure of **4a** (Figure S3) does not show π···π interactions.

The ^{1}H NMR spectra of **1a**–**6a** in $CDCl_3$ at room temperature, immediately after dissolving the corresponding solid brute or the crystalline material are consistent with the presence of four different molecules in solution. The resonances are associated with the presence of the new diplatinum complex (species **a**), with the starting material (**Pt-1**), the free ligand and, also the corresponding mononuclear complex with the dinucleating ligand acting as monodentate terminal group [Pt(pq)(C≡C^{t}Bu)(L-κ*N*)], (hereafter denoted as species **b**). Complete experimental data obtained for all systems are summarized in

the Experimental Section (labelling is shown in Scheme 1). As illustration, and for clarity, we only discuss the 4,4'-bpy complex (**2a**). The ^{1}H NMR spectra of the microcrystalline **2a** complex (B), the starting material **Pt-1** (C) and a mixture **Pt-1**:4,4'-bpy in 1:4 molar ratio (A) are presented in Figure 4. It should be noted that the coordination of the pyridine N atoms to the Pt center is supported by the well-known coordination-induced shifts of the α-H_{py} protons to downfield in relation to the free ligand (δ 8.75), which has been ascribed to the loss of electron density upon pyridine ring coordination. As seen in Figure 4B, only one signal appears at δ 9.00 (d), which is assigned to the bridging species **2a**, whereas the two expected different resonances located at 8.96 (d), 8.79 (d) correspond to the terminal species **2b**. This later signal (δ 8.79) lies close to that of the free bpy (δ 8.75), being therefore ascribed to the two α-H_{py} protons of the uncoordinated pyridine ring in **2b**. A particularly reliable indicator of the presence of starting material (**Pt-1**) is the signal H^8 of the pq ligand, very deshielded (δ 9.75) in relation to the others. Fortunately, in all systems under study, the pyridine protons (pyrazine for **1a**) and the H^8_{pq} signal of the **Pt-1** are sufficiently separated from the other signals, so they can be used to establish the approximate ratios from their integrations. Due to remarkable overlapping (or even coincidence for pq signals) an accurate assignment for the rest of signals to individual complexes is not possible. These spectra are consistent with partial dissociation of the *N*-bridging ligand at room temperature in $CDCl_3$, which could be driven by the *trans* labilizing effect of the *C*-cyclometalate atom on the *N*-donor ligand and the stability of the σ/π-C≡C^{t}Bu bridging system in the precursor **Pt-1**. A reasonable equilibrium (slow on the NMR scale) between the commented species is proposed in Scheme 2.

From a comparison of the analysis of the ^{1}H NMR spectra of these five bimetallic assemblies, we conclude that the experimental approximate ratio determined for the four species depend on the *N*-donor ligand: (**a**:**Pt-1**:**b**:**N-N**) ≈ 1:13.1:6.2:8.9 pyz, 1:0.8:1.3:0.2 bpy, 1:0.4:0.9:0.1 bpa, 1:0.5:0.9:0.1 bpe, 1:0.9:1.4:0.2 bpac). The higher proportion of the bimetallic species (**a**) in solution was found with the more flexible and donor ligands (bpa, bpe), whereas the lowest was with the short and rigid pyrazine ligand being the order: bpa ≈ bpe > bpac ≈ bpy >> pyz. For complex **6**, signals due to coordinated and free α-H pyridine protons are also observed together with that of the H^8_{pq} proton of **Pt-1**. However, in this system the possible occurrence of stepwise decoordination of the cyclometalating Pt units cannot be excluded.

Equilibria can be influenced significantly by changing concentration, temperature or solvent. Therefore, an examination of these parameters is important to get a more complete picture of the complexes under study. As representative example, we discuss in detail only the results of the 4,4'-bpy system (**2**). The influence of the concentration was confirmed by recording the ^{1}H NMR spectra of **2a** at different concentrations in $CDCl_3$. As shown in Figure 5, dilution of a solution from a 6×10^{-3} to 1×10^{-3} M causes a progressive shift of the equilibria (i) and (ii) to the right, increasing the presence of **Pt-1**, **2b** and free 4,4'-bpy with concomitant decreasing of **2a**. By contrast, upon lowering the temperature to 218 K (Figure S4) the concentration of **2a** increases, whereas those of **Pt-1**, **2b** and free bpy decrease (**2a**:**Pt-1**:**2b**:**N-N** ratio, 298 K ≈ 1:0.8:1.3:0.2 to 218 K 1:0.4:0.8:0.1 for a solution 3×10^{-3} M in $CDCl_3$). These results clearly confirm that the three complexes and the free ligand are involved in a dynamic equilibrium. By using CD_3COCD_3 as solvent for **2a** the final ratio found was **a**:**Pt-1**:**b**:**N-N** ≈ 1:2.2:2.4:1.2 (Figure S5). Therefore, in this solvent not only the equilibria (i and ii) are shifted to the right in more extension to that observed in $CDCl_3$, but also the formation of **Pt-1** and bpy

(equilibrium i) was favored in relation to **2b** (ii). As was expected, the bimetallic (**a**)/mononuclear (**b**) ratio was also influenced by the concentration of the dinucleating *N-N* ligand. Thus, the ^{1}H NMR spectra recorded for solutions formed by a mixing of **Pt-1**/L (**L$_2$**–**L$_5$**) 1:4 in $CDCl_3$ (established by UV-vis, see below) show mainly the signals associated to the mononuclear species (**b**), together with the free ligand in excess and small amount of the bimetallic species (**a**) (**a**:**Pt-1**:**b**:**N-N** ratio ≈ 1:0:8:14, bpy system, Figure 4A. No signals associated with the starting material (**Pt-1**) are observed, indicating that the equilibria drawn in Scheme 2 are essentially shifted in counterclockwise in the presence of excess ligand. In the case of the pyrazine system, a large excess of ligand is required to eliminate completely the presence of the precursor (**Pt-1**:pyz ≈ 1:20), what is in good agreement with the greater amount of starting material observed when the solid **1a** is dissolved. It is worth noting that from these solutions only the binuclear complexes **1a**–**5a** and mixtures **1a**–**5a** /**1b**–**5b** could be isolated. Despite many attempts, we never got crystals out of any of the mononuclear complexes. However, the proton spectra obtained under these conditions (ratio **Pt-1**:**N-N** 1:4 for ligands **L$_2$**–**L$_5$** or 1:20 for **L$_1$**) have allowed us to carry out a reasonable assignment of the signals of the mononuclear complexes **1b**–**5b** (2D ^{1}H-^{1}H spectra). As the resonances of the starting material, the free ligands and the mononuclear complexes **1b**–**5b** were known, it has been also possible to identify and to assign with some certainty some characteristic signals observed for the solids **1a**–**5a** in $CDCl_3$ solution (see Experimental Section).

Figure 4. ^{1}H NMR spectra ($CDCl_3$, 400 MHz, 298 K, aromatic region) of: (**A**) Aliquot of a reaction mixture **Pt-1**/4,4'-bpy in a 1:4 molar ratio; (**B**) Microcrystalline sample of [{Pt(pq)(C≡C^{t}Bu)}$_2$(μ-4,4'-bpy)] (**2a**); (**C**) [Pt(pq)(μ−κC^{α}:η^2-C≡C^{t}Bu)]$_2$ (**Pt-1**).

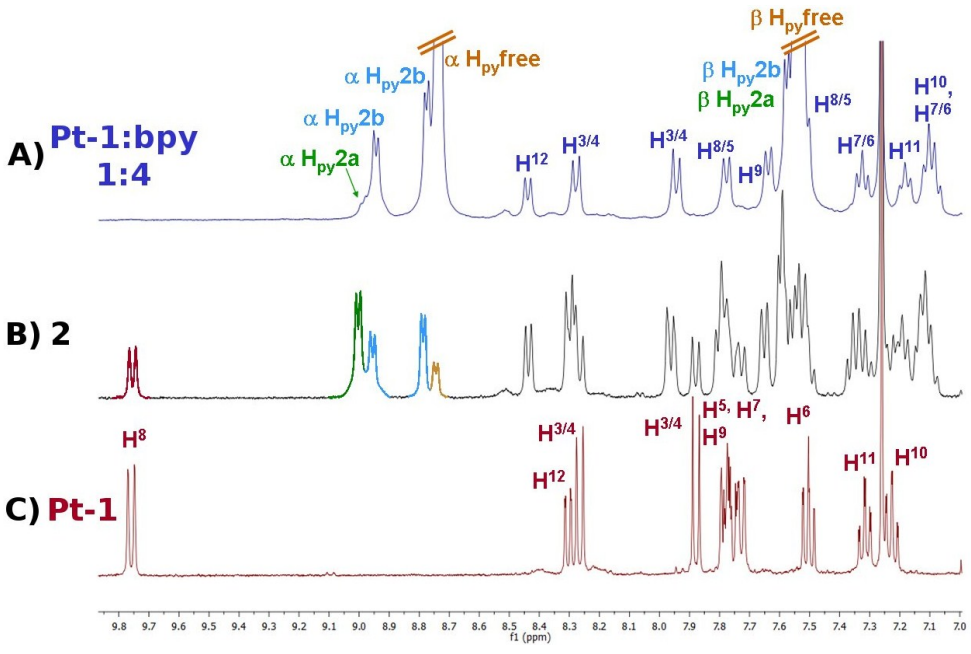

Scheme 2. Equilibrium proposed between the species **a**, **b**, **Pt-1** and the free ligand in systems **1**–**5**.

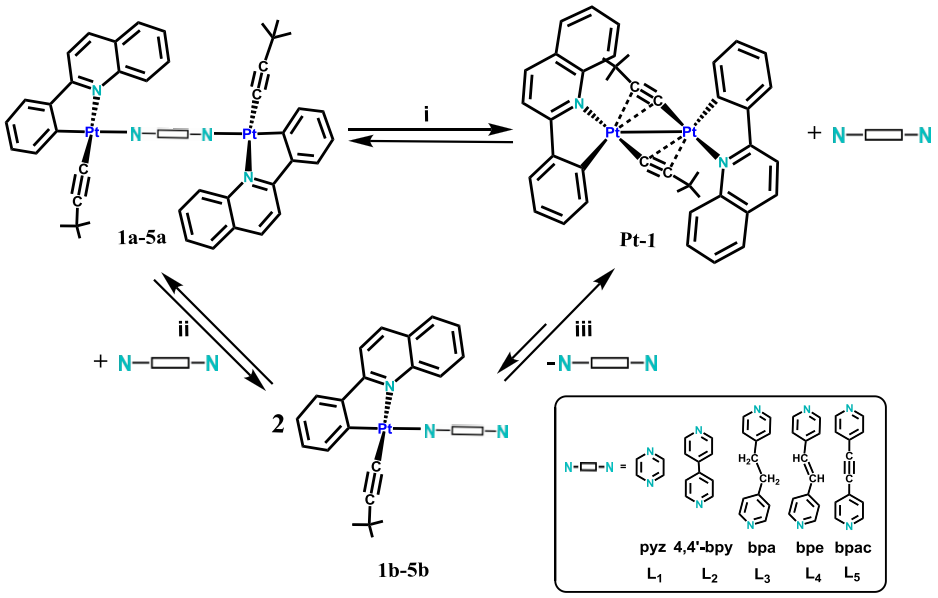

Figure 5. ^{1}H NMR spectra at 298 K of **2a** at different concentrations (mol/L). Selected resonances: **Pt-1** (*), **2a** (O), **2b** (Δ), free bpy (□).

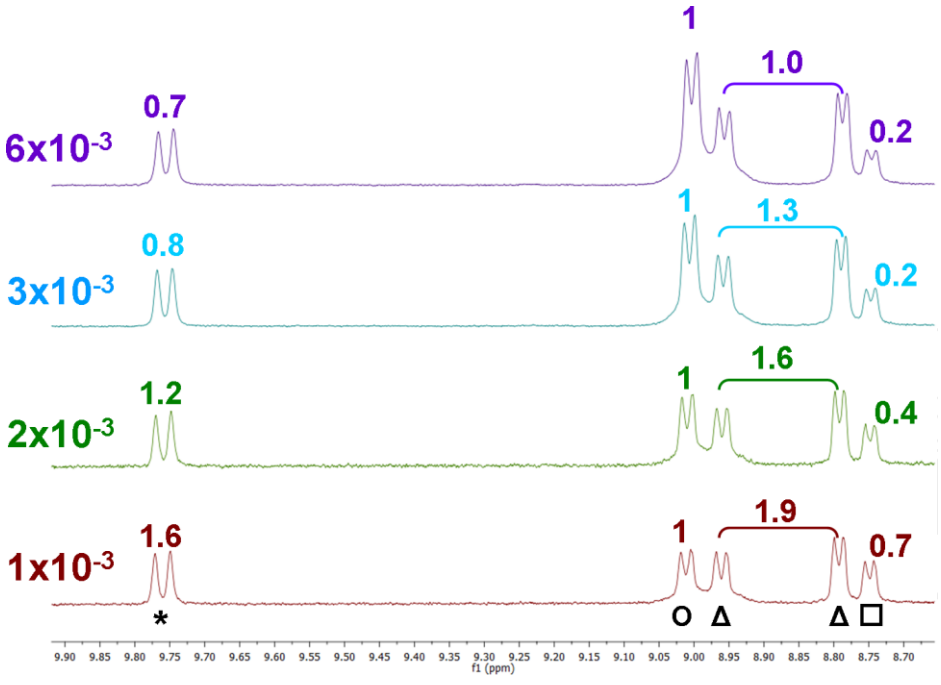

2.2. Photophysical Properties

To facilitate comparison, all absorption and emission spectral data are summarized in Tables 2 and 3.

Table 2. Absorption data for complexes **1a**–**6a** (solid state, diffuse reflectance) and for mixtures **Pt-1**:L (1:4) (**L_2**–**L_6**) and 1:14 (**L_1**) at 298 K (5×10^{-5} M CH_2Cl_2 solutions, see text).

Compounds	λ_{abs}/nm (10^3 ε M^{-1} cm^{-1})
1	242 (65.3), 276 (62.4), 304 (55.9), 353 (40.1), 408 (20.6) **CH_2Cl_2**
	300, 330, 365, 390, 430, 530 **solid**
2	243 (63.8), 270 (59.6), 341 (17.7), 354 (18.7), 410 (13.3) **CH_2Cl_2**
	305, 330, 355, 400, 500, 530 **solid**
3	218 (67.3), 257 (65.1), 299 (42.5), 337 (20.6), 355 (20.2), 413 (17.7) **CH_2Cl_2**
	300, 320, 350, 415, 525 **solid**
4	242 (63.3), 276 (63.9), 314 (58.3), 355 (29.9), 412 (20.7) **CH_2Cl_2**
	305, 345, 400, 425, 505, 535 **solid**
5	243 (63.3), 278 (62.2), 325(60.4), 355 (33.2), 410 (20.8) **CH_2Cl_2**
	305, 320, 360, 390, 420, 540 **solid**
6	245 (80.1), 289 (79.0), 308(71.7), 329_{sh} (43.9), 355 (35), 410 (6.0) **CH_2Cl_2**
	310, 360, 420, 545 tail to 630 **solid**

2.2.1. Absorption Spectroscopy

In the solid state, the diffuse reflectance of the polymetallic assemblies are characterized by a low energy and distinctive feature in the range 500–540 nm (with shoulder in **2a** and **4a**), which is absent in the precursor (Figure S6). According to TD-DFT in gas phase for **2a** (see below) this band is assigned to charge transfer from the Pt(pq)(C≡C^{t}Bu) units to the central *N*-*N* linker ^{1}[(M + L + L')L"CT].

As mentioned above, the ^{1}H NMR spectra of all complexes **1a**–**6a** in $CDCl_3$ solution are consistent with partial dissociation of the bridging ligand, establishing an equilibrium of the bimetallic complex (**a**) with starting material (**Pt-1**), the monometallic species (**b**) and the free ligand according to Scheme 2. Therefore, the obtained spectra are examined taking into account this behavior. The spectra of freshly prepared CH_2Cl_2 solutions of solid **1a**–**6a** show high energy features (240–330 nm) due to the intraligand transitions (pq, C≡CR and *N*-*N*-donor ligand). As is shown in Figure 6A for the 4,4'-bpy system, the intensity of these high energy bands exceeds that of the starting material (**Pt-1**), as expected for the occurrence of overlapping pyridyl ligand-centered transitions in this region (see Table S2 for absorption of the free ligands). The moderately structured band at 355 nm (**1**–**5**) coincides with that observed in the starting material **Pt-1**, being attributed to ^{1}IL (pq) charge transfer. However, the low-energy absorption (408–413 nm) appears remarkably blue-shifted in relation to the lowest manifold in the precursor, supporting cleavage of the double-alkynyl bridging system. In accordance with the NMR spectra commented before, the progressive addition of the corresponding *N*-*N*-donor ligand essentially causes the disappearance of **Pt-1**. By way of illustration, Figure 6B shows the spectra of the precursor (**Pt-1**), together with the changes observed upon successive addition of 4,4'-bpy. As it is observed, the maximum of the band is shifted to 410 nm with only 1 equiv. of ligand, but the band shows a long tail in the region where **Pt-1** still absorbs, thus confirming its presence. Upon addition of ca. 4 equiv. of ligand, the red-side of band decreases considerably, in accordance with the essentially disappearance of **Pt-1**. The band changes relatively little with additional equivalents of ligand, though upon addition of more ligand (6–30 equiv.), a small decreasing

of the tail is still observed. We attribute, tentatively, this latter change to a complete disappearance of bimetallic species (**a**) in solution, leaving mononuclear **b** complexes as the predominant metallic components. The fact that the stepwise addition of ligand takes place keeping the low energy maximum at 410 nm (with minor changes in the tail) suggests that the absorption profiles and electronic structures of bimetallic (species **a**) and mononuclear complexes (species **b**) are likely rather similar. A similar behavior has been previously observed in related systems [49]. In the case of the pyz-system, the low energy absorption band shows a gradual change and we determine a relation of *ca*. 1:14 as the point where the precursor essentially disappears, what is also in agreement with a greater dissociation of the *N*-ligand in the assembly. As is shown in Figure 6C, the ancillary *N*-*N* ditopic ligand has little influence in the low energy manifold. On the basis of previous spectroscopic investigations in phenylquinolyl and alkynyl platinum complexes [57], the low energy absorption band is tentatively ascribed to admixture of platina/alkynyl to cyclometalate (pq) charge transfer [d(Pt)/C≡C→π*(pq)] ^{1}[(M + L')LCT]. This assignment is in agreement with the slight blue shift observed for the less electron donating pyrazine ligand (408 nm) and the slightly red shift seen for the most electron donating 1,2-bis(4-pyridyl)ethane (bpa, 413 nm). However, due to the low lying nature of some of the π* diimine ligands, contribution from platina-alkynyl to *N*-donor ligand charge transfer ^{1}[Pt(C≡C)→π*(*N*-donor)] could be also plausible. This contribution is apparent in the bpac system (**5**), which displays enhanced absorption in the low energy tail (line rose).

2.2.2. Emission Spectroscopy

Qualitatively, the emissions of these complexes are much more intense in all media than those observed for the starting materials (Tables 3 and S3). The emission profiles are excitation-wavelength independent, indicating that aggregates are not responsible for the observed spectra. The emission spectra of **1a**–**6a** in solid state at room and at 77 K are shown in Figure 7. At room temperature, the bands are unstructured and maximize in the range 590–615 nm, whereas at low temperature the profiles become structured and slightly blue shifted. The decays for these solids were adequately modeled by a single exponential function (τ 0.3–11.4 μs 298 K; 7.6–39.2 μs 77 K) in the range of microseconds, revealing their triplet parentage. In the bpe-bridged binuclear compound **4a**, the highly structured emission profile at low temperature, with peak maxima at 588, 648 and 702 nm, the observed vibronic spacing (close to that observed for the free ligand), and also the long lifetime (39.2 μs) are consistent with a predominantly bpe-centered ^{3}IL ^{3}(ππ)* excited state. However, the emission profiles of **1a** (pyz) and **2a** (bpy) are similar (590 nm 298 K; 572, 610 77 K **1a**, 574, 612 nm 77 K **2a**) and compares to those seen for typical phenylquinolyl platinum complexes (*i.e*., [Pt(pq){$H_2B(pz)_2$}] λ_{em} = 580, 610 nm) [58], what is consistent with emission from a ^{3}MLCT excited state likely mixed with alkynyl to pq charge transfer contribution (^{3}MLCT/^{3}L'LCT). For the remaining complexes (**3a**, **5a** and **6a**), the low temperature profiles are also similar to those of **1a** and **2a**, but the maxima are slightly red shifted in the **6a**(tpac) > **3a**(bpa) > **5a**(bpac), pointing to some contribution of the central *N*-linker ligand.

Figure 6. (**A**) Absorption spectra of **2a**, [Pt(pq)(μ-κC^{α}:η^2-C≡C^{t}Bu)]$_2$ (**Pt-1**) and free 4,4'-bpy in CH_2Cl_2; (**B**) Normalized absorption spectra in CH_2Cl_2 of [Pt(pq)(μ-κC^{α}:η^2-C≡C^{t}Bu)]$_2$ (**Pt-1**) and successive additions of 1, 2, 4, 6, 8 and 30 equiv. of 4,4'-bpy; (**C**) Low energy region of the absorption spectra of solids **1a**–**6a** and **Pt-1** in CH_2Cl_2.

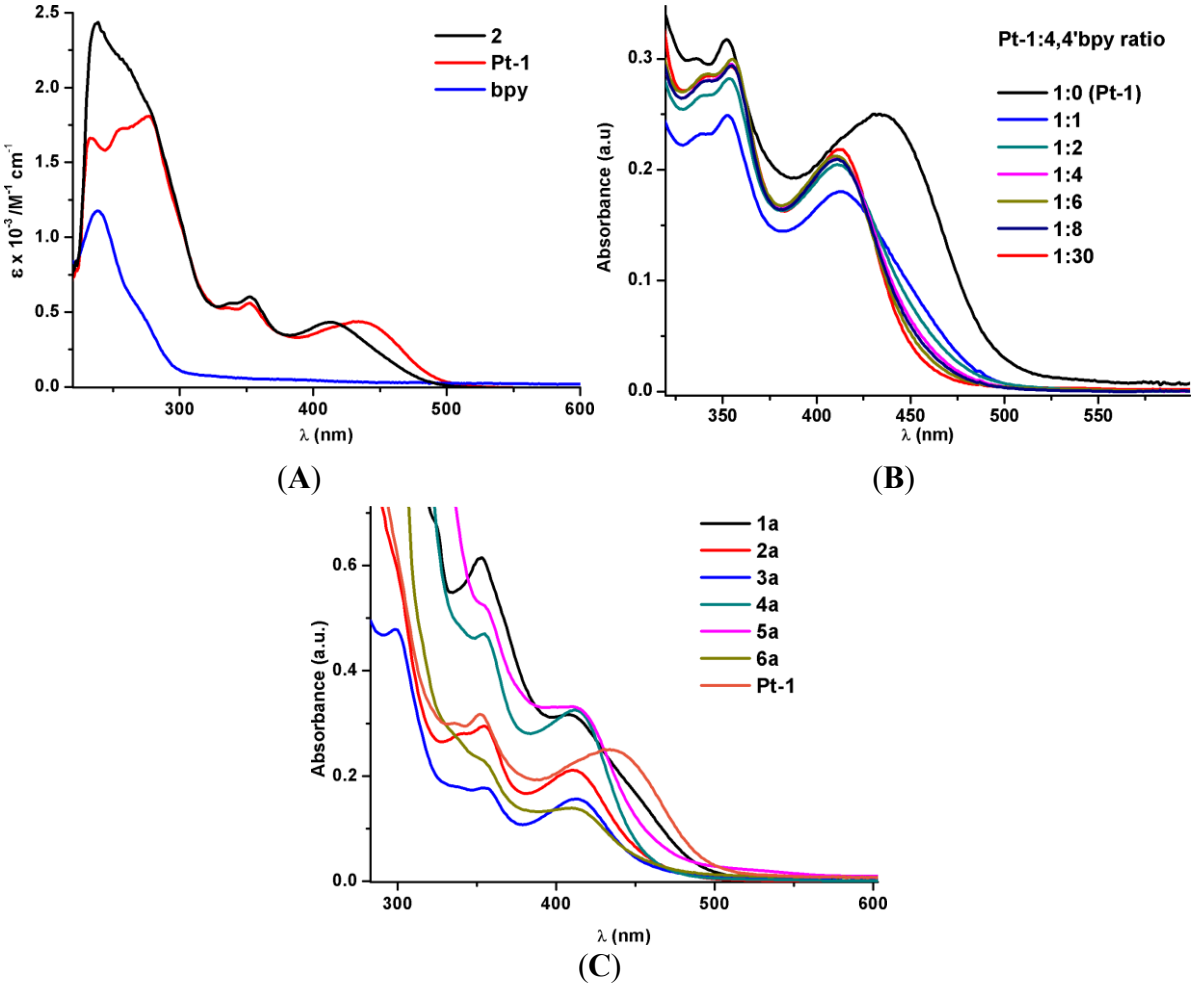

Figure 7. Normalized emission spectra of complexes **1a**–**6a** in solid state (**A**) at 298 K; (**B**) at 77 K (λ_{exc} 400 nm).

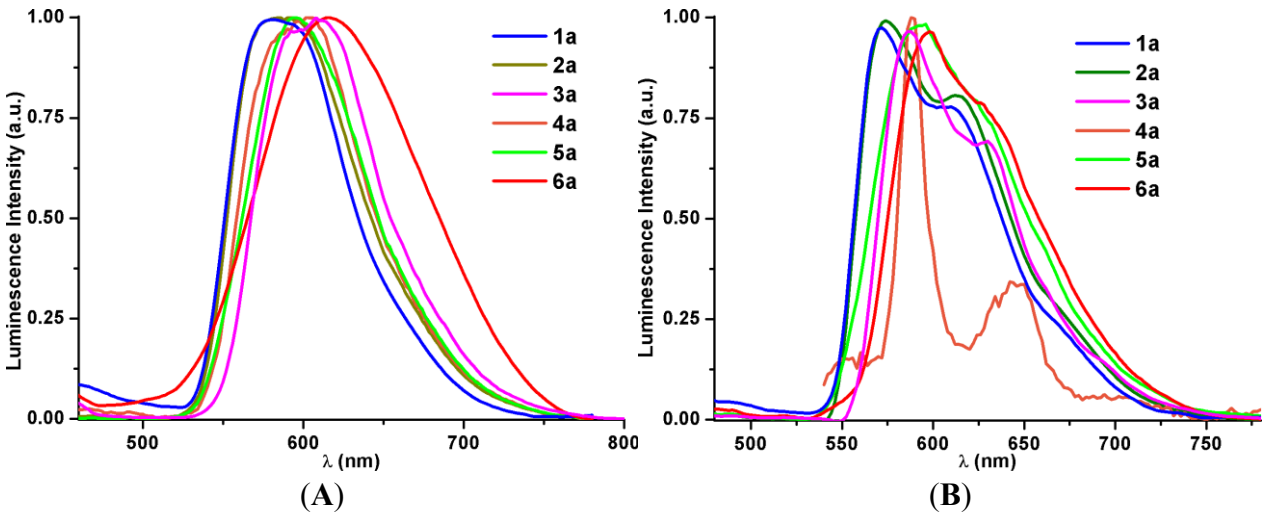

Table 3. Photophysical data for complexes **1a**–**6a** (solid state) and for mixtures **Pt-1**:L (1:4) (CH_2Cl_2, 5×10^{-5} M).

Compound	Medium (T [a]/K)	λ_{em}/nm (λ_{exc}/nm)	τ/μs	ϕ(%)
1	Solid (298)	590_{max} [a] (365–550)	8.0	13.8
	Solid (77)	572_{max}, 610, 660_{sh} (365–540)	14.0	-
	5×10^{-5} M (298)	595_{max} [a] (350–420)	-	-
	5×10^{-5} M (77)	570_{max}, 610, 660_{sh} (365–450)	-	-
2	Solid (298)	590 [a] (365–530)	9.9	13.1
	Solid (77)	574_{max}, 612, 650 (365–530)	12.2	-
	5×10^{-5} M (298)	590 [a] (365–410)	-	-
	5×10^{-5} M (77)	570_{max}, 625, 660_{sh} (365–430)	-	-
3	Solid (RT)	610[a] (365–540)	9.9	9.4
	Solid (77)	588_{max}, 625 (365–550)	7.7	-
	5×10^{-5} M (RT)	595 (365–420)	-	-
	5×10^{-5} M (77)	570_{max}, 610, 660_{sh} (365–460)	-	-
4	Solid (298)	605 [a] (365–540)	10.4	4.9
	Solid (77)	588_{max}, 648, 702 (365–540)	39.2	-
	5×10^{-5} M (77) [b]	578_{max}, 620, 650_{sh} (365–440)	13.8	-
5	Solid (298)	596 [a] (365–540)	11.4	6.8
	Solid (77)	596 [a] (365–540)	15.2	-
	5×10^{-5} M (298)	595 (365–420)	9.2	-
	5×10^{-5} M (77)	576_{max}, 613, 660_{sh} (365–440)	14.4	-
6	Solid (298)	615 [a] (365–500)	0.3	1.1
	Solid (77)	598 [a] (365–480)	7.6	-
	5×10^{-5} M (298)	595 (365–415)	-	-
	5×10^{-5} M (77)	570_{max}, 612, 670_{sh} (365–480)	-	-

[a] Tail to 800 nm; [b] Non emissive at 298 K.

Due to the occurrence of the dissociation process commented above, the study of the emissions in solution was carried out using CH_2Cl_2 solutions with a **Pt-1**:L proportion of 1:4 (data are listed in Table 3). Under these conditions, the predominant species in solution is the mononuclear complex (for **2b**–**5b**) or mixtures with the corresponding binuclear complex in the case of systems with pyrazine and the trinucleating 1,3,5-tris(pyridyl)acetylene ligand (**1** and **6**). As has been noted before, both species afford similar low energy absorption features. Not unexpectedly, the bpe complex (**4b**) is not emissive in fluid, probably due to easy nonradiative relaxation by forming a twisted triplet state (^{3}p) [49,59–61]. The remaining complexes display a rather similar intense broad emission centered around 595 nm with negligible influence of the *N*-donor auxiliary ligand, suggesting a similar emissive state (Figure 8A, Table 3). Upon cooling at 77 K, the emission shifts remarkably to higher energies exhibiting structured profiles (Figure 8B) with minimal variations in λ_{max} (range 570–576 nm). At 77 K, the bpe complex **4b** is also emissive (line orange) exhibiting similar structured profile with a peak maximum at 578 nm, pointing to a similar emissive state. In fact, lifetime measurements for two representative complexes with ligands bpe and bpac in glass state are also similar (see Table 3). The emission is mainly attributed to mononuclear complexes and it is ascribed to admixture of ^{3}MLCT and alkynyl to pq charge transfer (^{3}MLCT/^{3}L'LCT). Further support is obtained from the excitation spectra

in fluid solution, which resemble the corresponding absorption spectra in these conditions. Identical profiles but with reduced intensity are obtained from solution of binuclear **1a**–**3a** and **5a** solids (or by using **Pt-1**/L 1:1 molar ratio) likely due to similar luminescence response of the species **a** and **b** (both present in solution), which are clearly more emissive than the starting material. As illustration, the different spectra obtained for the **Pt-1**/bpy system in different molar ratio are shown in Figure S7. Interestingly, in contrast to the nonemissive behavior of the mononuclear complex **4b**, a diluted solution (5×10^{-5} M) of the bpe binuclear complex **4a** displays an unstructured band located at 600 nm upon excitation at 420 nm, which is related to the presence of the more rigid **4a** in solution. In glass, the band is only slightly structured and blue shift (565 max, 600 sh nm).

Figure 8. Emission spectra of mixtures (see text) of **Pt-1**:L (1:4 ratio) in CH_2Cl_2 (5×10^{-5} M) at (**A**) 298 K and (**B**) 77 K.

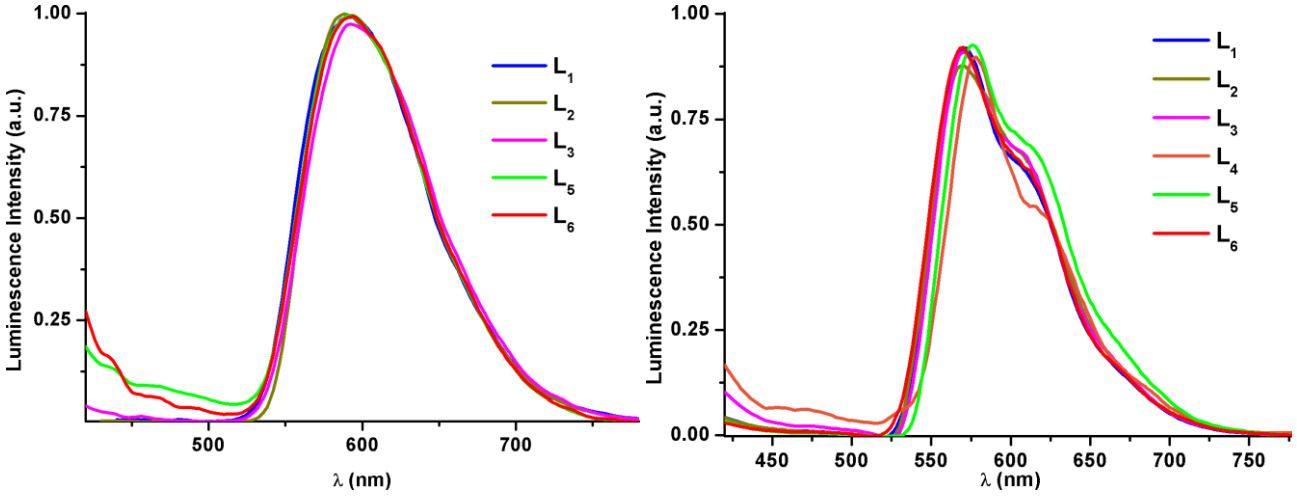

(**A**) (**B**)

2.3. Theoretical Calculations

To shed some light, TD-DFT and DFT calculations have been carried out for the species **2a**. The optimization in the ground state agrees well with the experimental structure (see Table S4 for details), the most remarkable difference being the lengthening of the Pt-*N*(pyridyl) distances. The distribution of the frontier molecular orbitals in the ground state and the corresponding partial molecular orbital composition (percentages), together with selected low-lying transitions in vacuum and in CH_2Cl_2 solution and the Cartesian coordinates are provided in Tables S5–S8. Some selected orbitals are shown in Figure 9. The HOMO and HOMO-1 have similar contribution from each one of the Pt and alkynyl units (*i.e.*, HOMO Pt (32%) and C≡C^{t}Bu (61%) on fragment 2; HOMO−1 Pt (35%) and C≡C^{t}Bu (57%) on fragment 1), whereas the HOMO−2 and HOMO−3 are of similar energy and located on the unit 2 Pt(pq)(C≡C^{t}Bu). The HOMO−4 is centered on fragment 1 [Pt (30%), pq (55%) and C≡C^{t}Bu (13%)]. The LUMO is mainly centered on the bipyridine ligand (94%) but the two following low lying virtual orbitals LUMO+1 and LUMO+2 are, however, localized on the low lying pq goups (LUMO+1 93%; LUMO+2 93%). The lowest energy absorption calculated in phase gas at 494 nm (Table S6) compares to that seen in the experimental solid reflectance spectrum at 530 nm. This band arises mainly from the HOMO−4 to LUMO transition and can be described to charge transfer from the Pt(pq)(C≡C^{t}Bu) units

of the fragment 1 to the central *N*-*N* linker ^{1}[(M + L + L')L"CT]. The two following excitations calculated around 482 nm are of more complex configuration with significant charge transfer from HOMO and HOMO−1 to LUMO+1 and LUMO+2. These absorptions are mainly ascribed to platinum-alkynyl to cyclometalated ^{1}[(M + L')LCT] and could be correlated with the experimental feature located at 500 nm.

Figure 9. Molecular orbital plots for the computed S_0 state of complex **2a** (Pt(2) **left**; Pt(1) **right**).

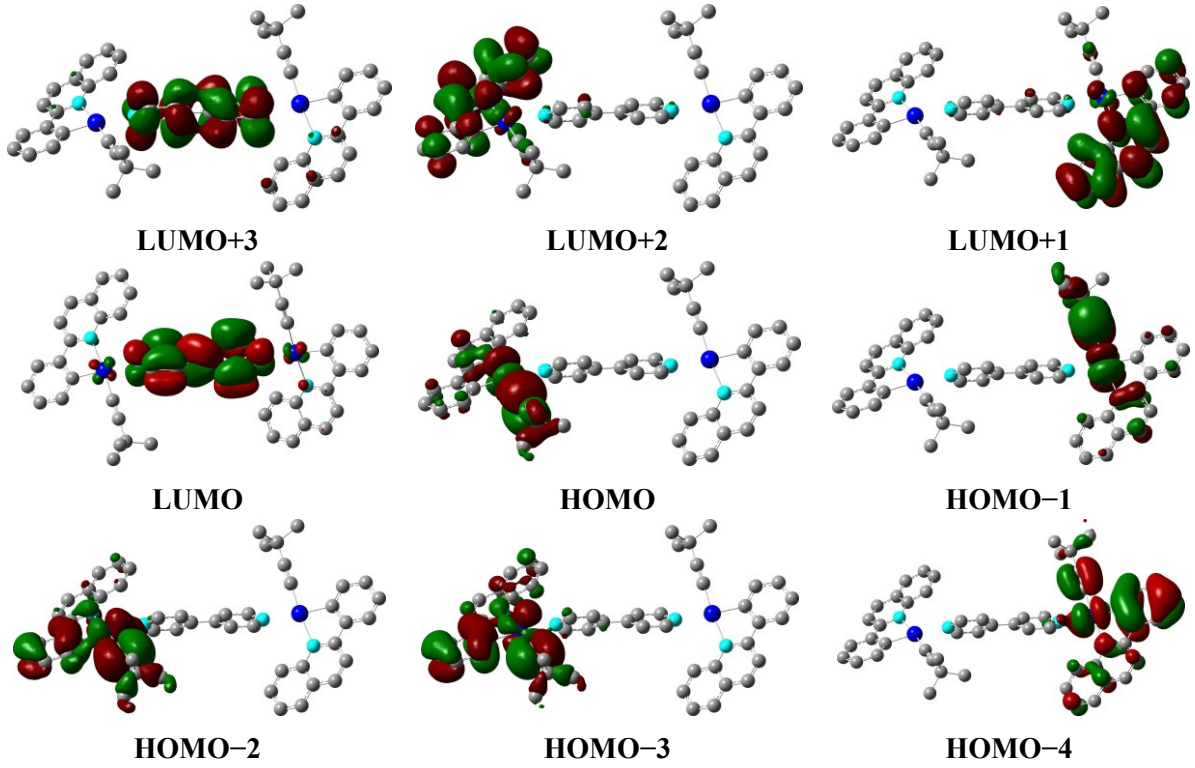

By taking into consideration the solvent (CH_2Cl_2), there is an obvious blue shift in the lowest singlet excitations in agreement with the nature of its charge transfer (Table S7). Interestingly, the transition which involves charge transfer to the central bpy linker (HOMO−4 to LUMO) now has higher energy (S_4, calculated at 419 nm). The three lower energy singlets (S_1, S_2 and S_3) have similar energy values (435, 431 and 428 nm) and are mainly composed of excitations from HOMO−3 to HOMO→LUMO to LUMO+2. Therefore, the experimental band located in solution at 410 nm could be ascribed as an admixture of platinum-alkynyl-pq to pq charge transfer ^{1}[(M + L + L')LCT] with contribution to the central bpy linker ^{1}[(M + L + L')L"CT] (L = pq, L' = C≡C^{t}Bu, L" = bpy).

To clarify the emission character of **2a**, its triplet state geometry in gas phase was optimized (Table S9). The calculated emission as the energy difference between S_0 and T_1 states (584 nm) is in accordance with the experimental value (590 nm). The excitation takes place with clear changes in the frontier orbitals respect to the ground state. The SOMO−1 is now located on the pq (58%), Pt (26%) and the alkynyl ligand (16%) on fragment 1, whereas the SOMO is mainly centered in the pq(1) (92%) (Figure 10). In agreement, the localization of the spin density lies on one of the pq ligands and the platinum/alkynyl group of one fragment of the molecule (Figure S8). Thus, the emission has a mixed platinum/alkynyl to phenylquinolyl charge transfer character ^{3}[(M + L')LCT] with some minor ^{3}IL(pq) contribution, supporting the negligible influence of the *N*-donor linker.

Figure 10. Molecular orbital plots for the computed T_1 state of complex **2a**.

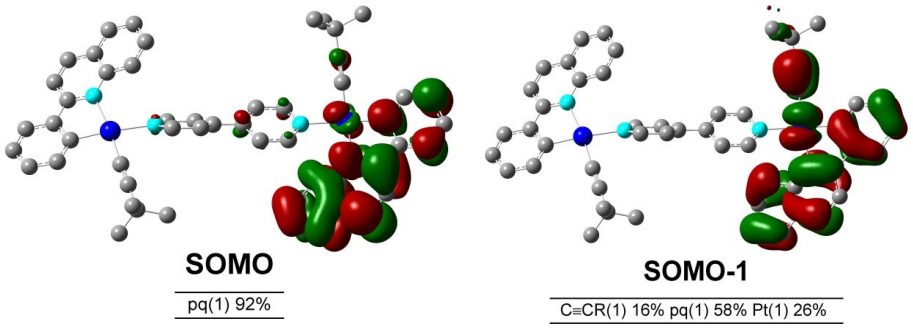

3. Experimental Section

General Comments. All reactions were carried out under an atmosphere of dry argon, using standard Schlenk techniques. Solvents were obtained from a solvent purification system (M-BRAUN MB SPS-800, MBRAUN, Garching, Germany). NMR spectra were recorded at 293 K on Bruker ARX 300 or ARX 400 spectrometers (Madison, WI, USA). Chemical shifts are reported in ppm relative to external standards ($SiMe_4$) and all coupling constants are given in Hz. The NMR spectral assignments of the phenylquinolyl ligands (Hpq) follow the numbering scheme shown in Scheme 1. IR spectra were obtained on a Nicolet Nexus FT-IR Spectrometer (Thermo Scientific, Waltham, UK), using KBr pellets. Elemental analyses were carried out with a Carlo Erba EA1110 CHNS-O microanalyzer (Carlo Erba, Rodano, Italy). Mass spectra were recorded on a HP-5989B mass spectrometer (Hewlett Packard, East Lyme, CT, USA) using the ES techniques (exact mass). The optical absorption spectra were recorded using a Hewlett-Packard 8453 (solution) spectrophotometer (Hewlett Packard, East Lyme, CT, USA) in the visible and near-UV ranges. Diffuse reflectance UV-vis (DRUV) data of pressed powder diluted with SiO_2 were recorded on a Shimadzu (UV-3600 spectrophotometer with a Harrick Praying Mantis accessory, Harrick Scientific Products, New York, NY, USA) and recalculated following the Kubelka-Munk function. Emission and excitation spectra were obtained on a Jobin-Yvon Horiba Fluorolog 3-11 Tau-3 spectrofluorimeter (Horiba, Kyoto, Japan), with the lifetimes measured in phosphorimeter mode (**6a** in solid state at 298 K was measured using a Data station HUB-B with a nanoLED controller DAS6). Quantum yields in solid state were measured upon excitation at ~400 nm using a F-3018 Integrating Sphere mounted on a Fluorolog 3-11 Tau-3 spectrofluorimeter (Horiba, Kyoto, Japan). The starting material $[Pt(pq)(\mu\text{-}\kappa C^{\alpha}\text{:}\eta^2\text{-}C{\equiv}C^tBu)]_2$ **(Pt-1)** [57] and the ligands di(4-pyridyl)acetylene [62] and 1,3,5-tris(pyridine-4-ylethynyl)benzene [63] were prepared according to the reported procedure.

Preparation of [{Pt(pq)(C≡C^{t}Bu)}$_2$(μ-pyz)] (1a). A solution of $[Pt(pq)(\mu\text{-}\kappa C^{\alpha}\text{:}\eta^2\text{-}C{\equiv}C^tBu)]_2$ (0.100 g, 0.104 mmol) in CH_2Cl_2 (20 mL) was treated with pyrazine (pyz) (0.017 g, 0.208 mmol) and the mixture was stirred for 3h. Evaporation to small volume (2 mL) afforded **1a** as an orange solid, which was filtered and washed with *n*-hexane (5 mL) (0.089 g, 82%). Anal. Calcd for $C_{46}H_{42}N_4Pt_2$ (1041.01): C, 53.07; H, 4.07; N, 5.38. Found: C, 53.32; H, 4.11; N, 5.12. ESI (+): *m*/*z* (%) 481 (77) $[Pt(pq)(C{\equiv}C^tBu)]^+$, 879 (41) $[Pt_2(pq)_2(C{\equiv}C^tBu)]^+$, 961 (100) $[\{Pt(pq)(C{\equiv}C^tBu)\}_2]^+$, 1041 (7) $[M]^+$. IR (KBr) (cm^{-1}): υ(C≡C) 2110 (m). ^1H NMR (δ, 300.13 MHz, $CDCl_3$) (**1a**:**Pt-1**:**1b**:**free ligand**, ~1:13.1:6.2:8.9): 9.75 (d, $J_{H\text{-}H}$ = 8.6, H^8_{pq} **Pt-1**), 8.90–8.84 (m, H^{α}_{pyz} **1a**, H^{α}_{pyz} **1b**), 8.63 (s, H^{α}_{pyz} **1b**),

8.60 (s, H^{α}_{pyz} **free**), 8.42 (d, $J_{H\text{-}H}$ = 7.4, H^{12}_{pq} **1a**, **1b**), 8.30 (d, $J_{H\text{-}H}$ = 7.5, H^{12}_{pq} **Pt-1**, $H^{3/4}_{pq}$ **1a**, **1b**), 8.27 (d, $J_{H\text{-}H}$ = 8.9, $H^{3/4}_{pq}$ **Pt-1**); 7.96 (d, $J_{H\text{-}H}$ = 8.0, $H^{3/4}_{pq}$ **1a**, **1b**), 7.89 (d, $J_{H\text{-}H}$ = 8.7, $H^{3/4}_{pq}$ **Pt-1**), 7.80–7.72 (m, $H^{8/5}_{pq}$ **1a**, **1b**; H^{7}_{pq}, H^{5}_{pq}, H^{9}_{pq} **Pt-1**), 7.65 (d, $J_{H\text{-}H}$ = 6.5, H^{9}_{pq} **1a**, **1b**), 7.51 (t, $J_{H\text{-}H}$ = 7.1, H^{6}_{pq} **Pt-1**), 7.49–7.29 (m, $H^{8/5}_{pq}$, $H^{7/6}_{pq}$ **1a**, **1b**; H^{11}_{pq} **Pt-1**), 7.34 (t, $J_{H\text{-}H}$ = 8.1, H^{11}_{pq} **Pt-1**), 7.23–7.12 (m, H^{11}_{pq}, H^{10}_{pq}, $H^{7/6}_{pq}$ **1a**, **1b**; H^{10}_{pq} **Pt-1**); 1.28 (s, H_{CH_3} **1a**, **1b**), 0.96 (s, H_{CH_3} **Pt-1**).

Data of the **Pt-1**:**pyz**, 1:20: (**1a**:**Pt-1**:**1b**:**free ligand**, ~1:0:7:82). ^{1}H NMR (δ, 400.17 MHz, **$CDCl_3$**): 8.83 (s, H^{α}_{pyz} **1a**); 8.81 (s, H^{α}_{pyz} **1b**), 8.59 (s, H^{α}_{pyz} **1b**, H^{α}_{pyz} **free**), 8.38 (d, $J_{H\text{-}H}$ = 7.9, H^{12}_{pq} **1a**, **1b**), 8.29 (d, $J_{H\text{-}H}$ = 8.5, $H^{3/4}_{pq}$ **1a**, **1b**), 7.94 (d, $J_{H\text{-}H}$ = 8.7, $H^{3/4}_{pq}$ **1a**, **1b**), 7.80 (d, $J_{H\text{-}H}$ = 7.9, $H^{8/5}_{pq}$ **1a**, **1b**), 7.63 (d, $J_{H\text{-}H}$ = 7.8, H^{9}_{pq} **1a**, **1b**), 7.39–7.35 (m, $H^{8/5}_{pq}$, $H^{7/6}_{pq}$ **1a**, **1b**), 7.20–7.09 (m, H^{11}_{pq}, $H^{7/6}_{pq}$, H^{10}_{pq} **1a**, **1b**), 1.27 (s, H_{CH_3} **1a**, **1b**).

Preparation of [{Pt(pq)(C≡C^{t}Bu)}$_2$(μ-bpy)] (2a). A solution of [Pt(pq)(μ-κC^{α}:η^2-C≡C^{t}Bu)]$_2$ (0.100 g, 0.104 mmol) in CH_2Cl_2 (20 mL) was treated with 4,4'-bipyridine (0.016 g, 0.104 mmol) and the obtained solution was stirred for 2 h. Evaporation to small volume (2 mL) and treating with *n*-hexane (10 mL) afforded **2a** as an orange microcrystalline solid (0.073 g, 63%). Anal. Calcd for $C_{52}H_{46}N_4Pt_2$ (1117.14): C, 55.91; H, 4.15; N, 5.02. Found: 55.74; H, 3.93; N, 4.86. ESI (+): *m*/*z* (%) 481 (100) [Pt(pq)(C≡C^{t}Bu)]$^+$, 637 (6) [Pt(pq)(C≡C^{t}Bu)(bpy)]$^+$, 879 (10) [Pt$_2$(pq)$_2$(C≡C^{t}Bu)]$^+$, 961 (77) [{Pt(pq)(C≡C^{t}Bu)}$_2$]$^+$, 1117 (3) [M]$^+$. IR (KBr) (cm^{-1}): υ(C≡C) 2117 (m). ^{1}H NMR (δ, 400.17 MHz, $CDCl_3$) (**2a**:**Pt-1**:**2b**:**free ligand**, ~1:0.8:1.3:0.2): 9.75 (d, $J_{H\text{-}H}$ = 8.6, H^{8}_{pq} **Pt-1**), 9.00 (d, $J_{H\text{-}H}$ = 5.9, H^{α}_{bpy} **2a**), 8.96 (d, $J_{H\text{-}H}$ = 5.8, H^{α}_{bpy} **2b**), 8.79 (d, $J_{H\text{-}H}$ = 5.3, H^{α}_{bpy} **2b**), 8.75 (d, $J_{H\text{-}H}$ = 5.1, H^{α}_{bpy} **free**), 8.44 (d, $J_{H\text{-}H}$ = 7.4, $J_{Pt\text{-}H}$ = 67.6, H^{12}_{pq} **2a**, **2b**), 8.30 (d, $J_{H\text{-}H}$ = 8.4, H^{12}_{pq} **Pt-1**, $H^{3/4}_{pq}$ **2a**, **2b**), 8.27 (d, $J_{H\text{-}H}$ = 9.8, $H^{3/4}_{pq}$ **Pt-1**), 7.96 (d, $J_{H\text{-}H}$ = 8.8, $H^{3/4}_{pq}$ **2a**, **2b**), 7.88 (d, $J_{H\text{-}H}$ = 8.6, $H^{3/4}_{pq}$ **Pt-1**), 7.79 (m, $H^{8/5}_{pq}$ **2a**, **2b**; H^{7}_{pq}, H^{5}_{pq} **Pt-1**), 7.73 (d, $J_{H\text{-}H}$ = 7.9, H^{9}_{pq} **Pt-1**), 7.65 (d, $J_{H\text{-}H}$ = 7.7, H^{9}_{pq} **2a**, **2b**), 7.61–7.54 (m, H^{β}_{bpy} **2a**, H^{β}_{bpy} **2b**, H^{β}_{bpy} **free**), 7.54 (m, $H^{8/5}_{pq}$ **2**, H^{6}_{pq} **Pt-1**), 7.36 (t, $J_{H\text{-}H}$ = 7.8, $H^{7/6}_{pq}$ **2a**, **2b**), 7.34 (t, $J_{H\text{-}H}$ = 8.1, H^{11}_{pq} **Pt-1**), 7.20 (m, H^{11}_{pq} **2a**, **2b**, H^{10}_{pq} **Pt-1**), 7.12 (m, $H^{7/6}_{pq}$, H^{10}_{pq} **2a**, **2b**), 1.30 (s, H_{CH_3} **2a**, **2b**), 0.96 (s, H_{CH_3} **Pt-1**).

At 218 K, 3 × 10^{-3} M (**Pt-1**:**2a**:**2b**:**free ligand**, ~1:0.4:0.8:0.1).

^{1}H NMR (δ, 400.17 MHz, CD_3COCD_3, 3 × 10^{-3} M): (**2a**:**Pt-1**:**2b**:**free ligand**, ~1:2.2:2.4:1.2).

Data of the **Pt-1**:**bpy**, 1:4: (**2a**:**Pt-1**:**2b**:**free ligand**, ~1:0:8:14). ^{1}H NMR (δ, 400.17 MHz, $CDCl_3$): 9.00 (d, $J_{H\text{-}H}$ = 6.0, H^{α}_{bpy} **2a**), 8.94 (d, $J_{H\text{-}H}$ = 5.8, H^{α}_{bpy} **2b**), 8.78 (d, $J_{H\text{-}H}$ = 5.3, H^{α}_{bpy} **2b**), 8.74 (d, $J_{H\text{-}H}$ = 4.9, H^{α}_{bpy} **free**), 8.44 (d, $J_{H\text{-}H}$ = 7.5, $J_{Pt\text{-}H}$ = 67.6, 1H, H^{12}_{pq} **2a**, **2b**), 8.28 (d, $J_{H\text{-}H}$ = 8.6, $H^{3/4}_{pq}$ **2a**, **2b**), 7.94 (d, $J_{H\text{-}H}$ = 8.6, $H^{3/4}_{pq}$ **2a**, **2b**), 7.78 (d, $J_{H\text{-}H}$ = 7.8, $H^{8/5}_{pq}$ **2a**, **2b**), 7.64 (d, $J_{H\text{-}H}$ = 7.5, H^{9}_{pq} **2a**, **2b**), 7.58 (d, $J_{H\text{-}H}$ = 5.7, H^{β}_{bpy} **2b**), 7.55 (d, $J_{H\text{-}H}$ = 5.6, H^{β}_{bpy} **2b**), 7.53 (d, $J_{H\text{-}H}$ = 5.1, H^{β}_{bpy} **free**), 7.51 (d, $J_{H\text{-}H}$ = 7.7, $H^{8/5}_{pq}$ **2a**, **2b**), 7.32 (t, $J_{H\text{-}H}$ = 7.5, $H^{7/6}_{pq}$ **2a**, **2b**), 7.18 (t, $J_{H\text{-}H}$ = 7.1, H^{11}_{pq} **2a**, **2b**), 7.10 (t, $J_{H\text{-}H}$ = 7.1, $H^{7/6/10}_{pq}$ **2a**, **2b**), 7.08 (t, $J_{H\text{-}H}$ = 7.6, $H^{7/6/10}_{pq}$ **2a**, **2b**), 1.28 (s, H_{CH_3} **2a**, **2b**).

Preparation of [{Pt(pq)(C≡C^{t}Bu)}$_2$(μ-bpa)] (3a). This compound was prepared as an orange microcrystalline solid (0.100 g, 85%) in a similar way to **2a**, starting from [Pt(pq)(μ-κC^{α}:η^2-C≡C^{t}Bu)]$_2$ (0.100 g, 0.104 mmol) and bis(4-pyridine)ethane (0.018 g, 0.104 mmol), but treating with Et_2O (10 mL). Anal. Calcd for $C_{54}H_{50}N_4Pt$ (1141.33): C, 56.64; H, 4.40; N, 4.89. Found: 56.43; H, 4.31; N, 5.10. ESI (+): *m*/*z* (%) 481 (72) [Pt(pq)(C≡C^{t}Bu)]$^+$, 662 (4) [Pt(pq)(C≡C^{t}Bu)(bpa)]$^+$, 879 (50) [Pt$_2$(pq)$_2$(C≡C^{t}Bu)]$^+$, 961 (100) [{Pt(pq)(C≡C^{t}Bu)}$_2$]$^+$, 1145 (16) [M]$^+$. IR (KBr) (cm^{-1}): υ(C≡C) 2119 (m). ^{1}H NMR (δ, 400.17 MHz, $CDCl_3$) (**3a**:**Pt-1**:**3b**:**free ligand**, ~1:0.4:0.9:0.1):

9.75 (d, $J_{H\text{-}H}$ = 8.6, H^8_{pq} **Pt-1**), 8.74 (d, $J_{H\text{-}H}$ = 5.7, H^{α}_{py} **3a**), 8.69 (d, $J_{H\text{-}H}$ = 6.1, H^{α}_{py} **3b**), 8.52 (d, $J_{H\text{-}H}$ = 5.4, H^{α}_{py} **3b**), 8.50 (d, $J_{H\text{-}H}$ = 5.4, 1H, H^{α}_{py} **free**), 8.42 (d, $J_{H\text{-}H}$ = 7.5, $J_{Pt\text{-}H}$ = 61.6, H^{12}_{pq} **3a**, **3b**), 8.30 (d, $J_{H\text{-}H}$ = 7.6, H^{12}_{pq} **Pt-1**), 8.27 (d, $J_{H\text{-}H}$ = 8.7, $H^{3/4}_{pq}$ **3a**, **3b**, $H^{3/4}_{pq}$ **Pt-1**), 7.94 (d, $J_{H\text{-}H}$ = 8.7, $H^{3/4}_{pq}$ **3a**, **3b**), 7.88 (d, $J_{H\text{-}H}$ = 8.7, $H^{3/4}_{pq}$ **Pt-1**), 7.80–7.73 (m, $H^{8/5}_{pq}$ **3a**, **3b**; H^5_{pq}, H^7_{pq}, H^9_{pq} **Pt-1**), 7.64 (d, $J_{H\text{-}H}$ = 7.4, H^9_{pq} **3a**, **3b**), 7.53–7.45 (m, $H^{8/5}_{pq}$ **3a**, **3b**, H^6_{pq} **Pt-1**), 7.35–7.29 (m, $H^{7/6}_{pq}$ **3a**, **3b**, H^{11}_{pq} **Pt-1**), 7.22–7.16 (m, H^{11}_{pq} **3a**, **3b**, $H^{1\circ\circ}_{pq}$ **Pt-1**), 7.11 (d, $J_{H\text{-}H}$ = 5.4, H^{β}_{py} **3a**, H^{β}_{py}**3b**), 7.08–7.04 (m, H^{β}_{py} **3b**, H^{β}_{py} **free**), 7.00 (d, $J_{H\text{-}H}$ = 7.8, $H^{7/6}_{pq}$, $H^{1\circ\circ}_{pq}$ **3a**, **3b**), 3.03 (s, H_{CH_2} **3a**), 3.00 (s, H_{CH_2} **3b**), 2.98 (s, H_{CH_2} **free**), 1.28 (s, H_{CH_3} **3a**, **3b**), 0.96 (s, H_{CH_3} **Pt-1**).

Data of the **Pt-1**:**bpa**, 1:4: (**3a**:**Pt-1**:**3b**:**free ligand,** ~**1**:**0**:**6**:**9**). ^{1}H NMR (δ, 400.17 MHz, $CDCl_3$): 8.74 (d, $J_{H\text{-}H}$ = 6.3, H^{α}_{py} **3a**), 8.69 (d, $J_{H\text{-}H}$ = 6.3, H^{α}_{py} **3b**), 8.52 (d, $J_{H\text{-}H}$ = 5.4, H^{α}_{py} **3b**), 8.50 (d, $J_{H\text{-}H}$ = 5.4, 1H, H^{α}_{py} **free**), 8.42 (d, $J_{H\text{-}H}$ = 7.4, $J_{Pt\text{-}H}$ = 63.5, H^{12}_{pq} **3a**, **3b**), 8.26 (d, $J_{H\text{-}H}$ = 8.7, $H^{3/4}_{pq}$ **3a**, **3b**), 7.93 (d, $J_{H\text{-}H}$ = 8.8, $H^{3/4}_{pq}$ **3a**, **3b**), 7.77 (d, $J_{H\text{-}H}$ = 7.9, $H^{8/5}_{pq}$ **3a**, **3b**), 7.63 (d, $J_{H\text{-}H}$ = 7.3, H^9_{pq} **3a**, **3b**), 7.46 (d, $J_{H\text{-}H}$ = 8.9, $H^{8/5}_{pq}$ **3a**, **3b**), 7.33 (d, $J_{H\text{-}H}$ = 7.5, $H^{7/6}_{pq}$ **3a**, **3b**), 7.17 (d, $J_{H\text{-}H}$ = 7.1, H^{11}_{pq} **3a**, **3b**), 7.11 (d, $J_{H\text{-}H}$ = 7.0, H^{β}_{py} **3a**, H^{β}_{py} **3b**), 7.07 (d, $J_{H\text{-}H}$ = 4.1, H^{β}_{py} **3b**, H^{β}_{py} **free**); 7.00 (d, $J_{H\text{-}H}$ = 7.7, $H^{7/6}_{pq}$, H^{10}_{q} **3a**, **3b**), 3.03 (s, H_{CH_2} **3a**), 3.00 (s, H_{CH_2} **3b**), 2.98 (s, H_{CH_2} **free**), 1.27 (s, H_{CH_3} **3a**, **3b**).

Preparation of [{Pt(pq)(C≡C^{t}Bu)}$_2$(μ-bpe)] (4a). This compound was prepared as an orange solid (0.070 g, 59%) in a similar way to **2a**, starting from [Pt(pq)(μ-κC^{α}:η^2-C≡C^{t}Bu)]$_2$ (0.100 g, 0.104 mmol) and 1,2-di(4-pyridyl)ethylene (0.019 g, 0.104 mmol), precipitating in the reaction media. Anal. Calcd for $C_{54}H_{48}N_4Pt_2$ (1143.18): C, 56.74; H, 4.23; N, 4.90. Found: C, 56.59; H, 4.23; N, 4.87. ESI (+): *m*/*z* (%) 481 (100) [Pt(pq)(C≡C^{t}Bu)]$^+$, 663 (6) [Pt(pq)(C≡C^{t}Bu)(bpe)]$^+$, 879 (8) [Pt$_2$(pq)$_2$(C≡C^{t}Bu)]$^+$, 961 (90) [{Pt(pq)(C≡C^{t}Bu)}$_2$]$^+$, 1143 (3) [M]$^+$. IR (KBr) (cm^{-1}): υ(C≡C) 2115 (s). ^{1}H NMR (δ, 400.17 MHz, $CDCl_3$) (**4a**:**Pt-1**:**4b**:**free ligand**, ~**1**:**0.5**:**0.9**:**0.1**): 9.75 (d, $J_{H\text{-}H}$ = 8.5, H^8_{pq} **Pt-1**), 8.85 (d, $J_{H\text{-}H}$ = 5.4, H^{α}_{py} **4a**), 8.82 (d, $J_{H\text{-}H}$ = 4.9, H^{α}_{py} **4b**), 8.66 (d, $J_{H\text{-}H}$ = 4.9, 1H, H^{α}_{py} **4b**), 8.64 (d, $J_{H\text{-}H}$ = 4.7, 1H, H^{α}_{py} **free**), 8.43 (d, $J_{H\text{-}H}$ = 7.8, $J_{Pt\text{-}H}$ = 61.4, 1H, H^{12}_{pq} **4a**, **4b**), 8.31–8.26 (m, $H^{3/4}_{pq}$ **4a**, **4b**; H^{12}_{pq}, $H^{3/4}_{pq}$ **Pt-1**), 7.96 (d, $J_{H\text{-}H}$ = 8.6, $H^{3/4}_{pq}$ **4a**, **4b**), 7.89 (d, $J_{H\text{-}H}$ = 8.4, $H^{3/4}_{pq}$ **Pt-1**), 7.79 (d, $J_{H\text{-}H}$ = 7.9, $H^{8/5}_{pq}$ **4a**, **4b**; H^7_{pq}, H^5_{pq} **Pt-1**), 7.73 (d, $J_{H\text{-}H}$ = 8.0, H^9_{pq} **Pt-1**), 7.65 (d, $J_{H\text{-}H}$ = 7.4, H^9_{pq} **4a**, **4b**), 7.55–7.49 (m, $H^{8/5}_{pq}$ **4a**, **4b**, H^6_{pq} **Pt-1**), 7.42–7.37 (m, H^{β}_{py} **4a**, H^{β}_{py} **4b**, H^{β}_{py} **free**), 7.35–7.30 (m, $H^{7/6}_{pq}$ **4a**, **4b**, H^{11}_{pq} **Pt-1**), 7.26–7.19 (m, $H_{C=CH}$ **4a**, $H_{C=CH}$ **4b**, $H_{C=CH}$ **free**, H^{10}_{pq} **Pt-1**), 7.11 (d, $J_{H\text{-}H}$ = 7.0, $H^{7/6}_{pq}$, $H^{1\circ\circ}_{pq}$ **4a**, **4b**), 1.29 (s, H_{CH_3} **4a**, **4b**), 0.96 (s, H_{CH_3} **Pt-1**).

Data of the **Pt-1**:**bpe**, 1:4: (**4a**:**Pt-1**:**4b**:**free ligand**, ~1:0:5:8). ^{1}H NMR (υ, 400.17 MHz, $CDCl_3$): 8.83 (d, $J_{H\text{-}H}$ = 5.9, H^{α}_{py} **4a**), 8.81 (d, $J_{H\text{-}H}$ = 6.0, H^{α}_{py} **4b**), 8.65 (d, $J_{H\text{-}H}$ = 5.6, H^{α}_{py} **4b**), 8.63 (d, $J_{H\text{-}H}$ = 5.4, H^{α}_{py} **free**), 8.44 (d, $J_{H\text{-}H}$ = 7.3, $J_{Pt\text{-}H}$ = 62.0, H^{12}_{pq} **4a**, **4b**), 8.28 (d, $J_{H\text{-}H}$ = 8.7, $H^{3/4}_{pq}$ **4a**, **4b**), 7.95 (d, $J_{H\text{-}H}$ = 8.7, $H^{3/4}_{pq}$ **4a**, **4b**), 7.78 (d, $J_{H\text{-}H}$ = 7.8, $H^{8/5}_{pq}$ **4a**, **4b**), 7.64 (d, $J_{H\text{-}H}$ = 7.6, H^9_{pq} **4a**, **4b**), 7.53 (d, $J_{H\text{-}H}$ = 8.7, $H^{8/5}_{pq}$ **4a**, **4b**), 7.40 (d, $J_{H\text{-}H}$ = 5.5, H^{β}_{py} **4b**), 7.39 (d, $J_{H\text{-}H}$ = 5.5, H^{β}_{py} **free**), 7.34 (t, $J_{H\text{-}H}$ = 7.6, $H^{7/6}_{pq}$ **4a**, **4b**), 7.32 (s, $H_{C=C}$ **4a**), 7.29 (s, $H_{C=C}$ **4b**), 7.23 (s, $H_{C=C}$ **4b**), 7.21 (s, $H_{C=C}$ **free**), 7.18 (t, $J_{H\text{-}H}$ = 8.3, H^{11}_{pq} **4a**, **4b**), 7.11 (t, $J_{H\text{-}H}$ = 7.5, $H^{7/6}_{pq}$, H^{10}_{pq} **4a**, **4b**), 1.29 (s, H_{CH_3} **4a**, **4b**).

Preparation of [{Pt(pq)(C≡C^{t}Bu)}$_2$(μ-bpac)] (5a). This compound was prepared as an orange microcrystalline solid (0.085 g, 72%) in a similar way to **1a**, starting from [Pt(pq)(μ-κC^{α}:η^2-C≡C^{t}Bu)]$_2$

(0.100 g, 0.104 mmol) and di(4-pyridyl)acetylene (0.038 g, 0.208 mmol), but it was stirred for 12 h. Anal. Calcd for $C_{54}H_{46}N_4Pt_2$ (1141.16): C, 56.84; H, 4.06; N, 4.91. Found: C, 56.47; H, 4.08; N, 4.78. ESI (+): *m/z* (%) 481 (100) $[Pt(pq)(C{\equiv}C^tBu)]^+$, 663 (6) $[Pt(pq)(C{\equiv}C^tBu)(bpac)]^+$, 879 (55) $[Pt_2(pq)_2(C{\equiv}C^tBu)]^+$, 961 (86) $[\{Pt(pq)(C{\equiv}C^tBu)\}_2]^+$, 1141 (3) $[M]^+$. IR (KBr) (cm^{-1}): $\upsilon(C{\equiv}C)_{(internal\ C{\equiv}C)}$ 2223 (w), $\upsilon(C{\equiv}C)$ 2118 (s). ^1H NMR (δ, 300.13 MHz, $CDCl_3$) (**5a**:**Pt-1**:**5b**:**free ligand**, ~1:0.9:1.4:0.2): 9.75 (d, $J_{H\text{-}H}$ = 8.6, $H^8{}_{pq}$ **Pt-1**), 8.89 (d, $J_{H\text{-}H}$ = 5.6, $H^{\alpha}{}_{py}$ **5a**), 8.86 (d, $J_{H\text{-}H}$ = 5.6, $H^{\alpha}{}_{py}$ **5b**), 8.68 (d, $J_{H\text{-}H}$ = 4.5, $H^{\alpha}{}_{py}$ **5b**), 8.66 (d, $J_{H\text{-}H}$ = 6.0, $H^{\alpha}{}_{py}$ **free**), 8.41 (d, $J_{H\text{-}H}$ = 7.0, $J_{Pt\text{-}H}$ = 62.3, $H^{12}{}_{pq}$ **5a**, **5b**), 8.31–8.26 (m, $H^{12}{}_{pq}$, $H^{3/4}{}_{pq}$ **Pt-1**, $H^{3/4}{}_{pq}$ **5a**, **5b**), 7.96 (d, $J_{H\text{-}H}$ = 8.6, $H^{3/4}{}_{pq}$ **5a**, **5b**), 7.89 (d, $J_{H\text{-}H}$ = 8.6, $H^{3/4}{}_{pq}$ **Pt-1**), 7.80–7.77 (m, $H^{8/5}{}_{pq}$ **5a**, **5b**; $H^7{}_{pq}$, $H^5{}_{pq}$ **Pt-1**), 7.73 (d, $J_{H\text{-}H}$ = 7.9, $H^9{}_{pq}$ **Pt-1**), 7.65 (d, $J_{H\text{-}H}$ = 7.2, $H^9{}_{pq}$ **5a**, **5b**), 7.53–7.48 (m, $H^{8/5}{}_{pq}$ **5a**, **5b**, $H^6{}_{pq}$ **Pt-1**), 7.41 (m, $H^{\beta}{}_{py}$ **5a**, $H^{\beta}{}_{py}$ **5b**, $H^{\beta}{}_{py}$ **free**), 7.39–7.32 (m, $H^{7/6}{}_{pq}$ **5a**, **5b**, $H^{11}{}_{pq}$ **Pt-1**), 7.19–7.09 (m, $H^{7/6}{}_{pq}$, $H^{11}{}_{pq}$, $H^{10}{}_{pq}$ **5a**, **5b**; $H^{10}{}_{pq}$ **Pt-1**), 1.29 (s, H_{CH_3} **5a**, **5b**), 0.96 (s, H_{CH_3} **Pt-1**).

Data of the **Pt-1**:**bpac**, 1:4: (**5a**:**Pt-1**:**5b**:**free ligand**, ~1:0:4:7). ^1H NMR (δ, 400.17 MHz, $CDCl_3$): 8.90 (d, $J_{H\text{-}H}$ = 5.9, $H^{\alpha}{}_{py}$ **5a**), 8.87 (d, $J_{H\text{-}H}$ = 6.4, $H^{\alpha}{}_{py}$ **5b**), 8.68 (d, $J_{H\text{-}H}$ = 5.8, $H^{\alpha}{}_{py}$ **5b**), 8.66 (d, $J_{H\text{-}H}$ = 5.8, $H^{\alpha}{}_{py}$ **free**), 8.44 (d, $J_{H\text{-}H}$ = 6.1, $H^{12}{}_{pq}$ **5a**, **5b**), 8.29 (d, $J_{H\text{-}H}$ = 8.2, $H^{3/4}{}_{pq}$ **5a**, **5b**), 7.95 (d, $J_{H\text{-}H}$ = 8.8, $H^{3/4}{}_{pq}$ **5a**, **5b**), 7.80 (d, $J_{H\text{-}H}$ = 8.0, $H^{8/5}{}_{pq}$ **5a**, **5b**), 7.65 (d, $J_{H\text{-}H}$ = 7.7, $H^9{}_{pq}$ **5a**, **5b**), 7.50 (d, $J_{H\text{-}H}$ = 9.7, $H^{8/5}{}_{pq}$ **5a**, **5b**), 7.42 (d, $J_{H\text{-}H}$ = 7.2, $H^{\beta}{}_{py}$ **5a**, **5b**), 7.41 (d, $J_{H\text{-}H}$ = 5.9, $H^{\beta}{}_{py}$ **5b**, **free**), 7.36 (t, $J_{H\text{-}H}$ = 7.0, $H^{7/6}{}_{pq}$ **5a**, **5b**), 7.21-7.07 (m, $H^{7/6}{}_{pq}$, $H^{10}{}_{pq}$, $H^{11}{}_{pq}$ **5a**, **5b**), 1.30 (s, H_{CH_3} **5a**, **5b**).

Preparation of [{Pt(pq)(C≡C^{t}Bu)}$_3$(μ-tpab)] (6a). A solution of $[Pt(pq)(\mu\text{-}\kappa C^{\alpha}{:}\eta^2\text{-}C{\equiv}C^tBu)]_2$ (0.150 g, 0.156 mmol) in CH_2Cl_2 (20 mL) was treated with 1,3,5-tris(pyridine-4-ylethynyl)benzene (0.040 g, 0.104 mmol) (molar ratio 3:2) and the orange solution was stirred for 4 h. Evaporation to small volume (2 mL) and treating with *n*-hexane (5 mL) gave **6a** as an orange microcrystalline solid (0.152 g, 80%). Anal. Calcd for $C_{90}H_{72}N_6Pt_3$ (1822.87): C, 59.30; H, 3.98; N, 4.61. Found: C, 59.19; H, 3.92; N, 4.40. ESI (+): *m/z* (%) 879 (51) $[Pt_2(pq)_2(C{\equiv}C^tBu)]^+$, 961 (100) $[\{Pt(pq)(C{\equiv}C^tBu)\}_2]^+$, 1342 (21) $[Pt_2(pq)_2(C{\equiv}C^tBu)_2L]^+$, 1660 (3) $[M\text{-}2C{\equiv}C^tBu]^+$, 1823 (2) $[M]^+$. IR (KBr) (cm^{-1}): $\upsilon(C{\equiv}C)_{(internal\ C{\equiv}C)}$ 2212 (m), $\upsilon(C{\equiv}C)$ 2115 (m). ^1H NMR (δ, 300.13 MHz, $CDCl_3$): 9.75 (d, $J_{H\text{-}H}$ = 8.6, $H^8{}_{pq}$ **Pt-1**), 8.85 (m, $H^{\alpha}{}_{py}$ **6a**, $H^{\alpha}{}_{py}$ **6b**), 8.65 (m, $H^{\alpha}{}_{py}$ **6b**, $H^{\alpha}{}_{py}$ **free**), 8.42 (d, $J_{H\text{-}H}$ = 8.3, $H^{12}{}_{pq}$ **6a**, **6b**, **6c**), 8.30 (d, $J_{H\text{-}H}$ = 7.3, $H^{12}{}_{pq}$ **Pt-1**, $H^{3/4}{}_{pq}$ **6a**, **6b**, **6c**), 8.27 (d, $J_{H\text{-}H}$ = 7.9, $H^{3/4}{}_{pq}$ **Pt-1**), 7.96 (d, $J_{H\text{-}H}$ = 8.3, $H^{3/4}{}_{pq}$ **6a**, **6b**, **6c**), 7.89 (d, $J_{H\text{-}H}$ = 8.8, $H^{3/4}{}_{pq}$ **Pt-1**), 7.80–7.72 (m, $H^{8/5}{}_{pq}$ **6a**, **6b**, **6c**; $H^7{}_{pq}$, $H^5{}_{pq}$, $H^9{}_{pq}$ **Pt-1**, $H^{\beta}{}_{py}$ **6a**, C-$H_{C_6H_3}$ **6a**, C-$H_{C_6H_3}$ **6b**, C-$H_{C_6H_3}$ **free**), 7.66-7.62 (m, $H^9{}_{pq}$ **6**, $H^{\beta}{}_{py}$ **6b**,), 7.53–7.49 (m, $H^{8/5}{}_{pq}$ **6a**, **6b**, **6c**, $H^6{}_{pq}$ **Pt-1**), 7.39–7.42 (m, $H^{\beta}{}_{py}$ **free**, $H^{7/6}{}_{pq}$ **6a**, **6b**, **6c**, $H^{11}{}_{pq}$ **Pt-1**), 7.19–7.10 (m, $H^{7/6}{}_{pq}$, $H^{11}{}_{pq}$, $H^{10}{}_{pq}$ **6a**, **6b**, **6c**; $H^{10}{}_{pq}$ **Pt-1**), 1.30 (s, H_{CH_3} **6a**, **6b**, **6c**), 0.96 (s, H_{CH_3} **Pt-1**).

Data of the **Pt-1**:**tpab**, 1:4. ^1H NMR (δ, 400.17 MHz, $CDCl_3$): 8.85 (d, $J_{H\text{-}H}$ = 4.6, $H^{\alpha}{}_{py}$ **6a**), 8.81 (d, $J_{H\text{-}H}$ = 4.8, $H^{\alpha}{}_{py}$ **6b**), 8.64 (d, $J_{H\text{-}H}$ = 4.2, $H^{\alpha 2}{}_{py}$ **6b**, $H^{\alpha}{}_{py}$ **free**), 8.42 (d, $J_{H\text{-}H}$ = 7.4, $H^{12}{}_{pq}$ **6a**, **6b**, **6c**), 8.29 (d, $J_{H\text{-}H}$ = 8.6, $H^{3/4}{}_{pq}$ **6a**, **6b**, **6c**), 7.95 (d, $J_{H\text{-}H}$ = 8.6, $H^{3/4}{}_{pq}$ **6a**, **6b**, **6c**), 7.82–7.79 (m, $J_{H\text{-}H}$ = 8.0, $H^{8/5}{}_{pq}$ **6a**, **6b**, **6c**, $H^{\beta}{}_{py}$ **6a**), 7.78 (s, C-$H_{C_6H_3}$ **6a**), 7.76 (s, C-$H_{C_6H_3}$ **6b**), 7.75 (s, C-$H_{C_6H_3}$ **free**), 7.64 (d, $J_{H\text{-}H}$ = 7.9, $H^9{}_{pq}$ **6a**, **6b**, **6c**), 7.60 (d, $J_{H\text{-}H}$ = 5.4, $H^{\beta}{}_{py}$ **6b**), 7.51 (d, $J_{H\text{-}H}$ = 8.9, $H^{8/5}{}_{pq}$ **6a**, **6b**, **6c**), 7.40–7.37 (m, $H^{\beta}{}_{py}$ **free**, $H^{7/6}{}_{pq}$ **6a**, **6b**, **6c**), 7.20–7.09 (m, $H^{7/6}{}_{pq}$, $H^{10}{}_{pq}$, $H^{11}{}_{pq}$ **6a**, **6b**, **6c**), 1.30 (s, H_{CH_3} **6a**, **6b**, **6c**).

X-ray Crystallography: Details of the structural analyses for all complexes are summarized in Table S10. Orange (**2**, **4**) crystals were obtained by slow diffusion at room temperature of *n*-hexane

into solutions of the complexes in $CHCl_3$. In all the cases, graphite-monochromatic Mo-K_α radiation was used, X-ray intensity data were collected with a NONIUS-κCCD area-detector diffractometer (CAMCOR, Oregon, USA) and images processed using the DENZO (Academic Press: New York, NY, USA) and SCALEPACK suite of programs [64], carrying out the absorption correction at this point. The structures were solved by Direct and Patterson Methods using SIR2004 [65], and refined by full-matrix least squares on F^2 with SHELXL-97 [66]. All non-hydrogen atoms were assigned anisotropic displacement parameters. All the hydrogen atoms were constrained to idealized geometries fixing isotropic displacement parameters 1.2 times the U_{iso} value of their attached carbon. Finally, the structures show some residual peaks greater than 1 eA^{-3} in the vicinity of the platinum atoms, but with no chemical meaning. CCDC 1024492-1024493 contain the supplementary crystallographic data for compounds **2a**·$2CHCl_3$·C_6H_{14} and **4a**·$4CHCl_3$ [67].

Computational Details for Theoretical Calculations. DFT and TD-DFT calculations were performed on complex **2a** with Gaussian 03 revision E.01 [68]. Geometries in the S_0 ground state and T_1 excited state were optimized using the restricted B3LYP (S_0) or unrestricted U-B3LYP (T_1) Becke's three-parameter functional combined with Lee-Yang-Parr's correlation functional [69–71]. The basis set used for the platinum centers was the LanL2DZ effective core potential [72] and 6-31G(d,p) for the ligand atoms. The solvent effect of the dichloromethane in the TD-DFT calculation was taken into consideration by the polarizable continuum model (PCM) [73] using CPCM [74].

4. Conclusions

In this study, we present a series of different bidentate *N*-donor ligands of different lengths and flexibility and one *N*-tridentate ligand, which undergo bridge-splitting reactions with [Pt(pq)(μ-κC^α:η^2-C≡C^{t}Bu)]$_2$ (**Pt-1**) to form binuclear [{Pt(pq)(C≡C^{t}Bu)}$_2$(μ-L)] (**1a**–**5a**) and trinuclear [{Pt(pq)(C≡C^{t}Bu)}$_3$(μ-L)] (**6a**) derivatives. The structures of **2a** and **4a** have been confirmed by *X*-ray crystallography. Probably due to the *trans* labializing effect of the *C*-cyclometalating atom and the high stability of **Pt-1**, these complexes rearrange in solution giving rise to a dynamic equilibrium between the diplatinum complexes (**1a**–**5a**), the mononuclear species [Pt(pq)(C≡C^{t}Bu)(L-κ*N*)] (**1b**–**5b**), (**Pt-1**) and the free ligand (L), as confirmed by ^{1}H NMR experiments. The equilibrium is affected by the concentration, temperature and solvent polarity. The higher proportion of the bimetallic species (**a**) in solution was found with the more flexible and donor ligands (bpa, bpe), in concentrated solutions, at low temperatures and with less polar solvents.

TD-DFT calculations on **2a** allow to assign the low-energy absorption band in solid state to Pt(pq)(C≡C^{t}Bu) to *N*-linker charge transfer (500–540 nm) ^{1}[(M + L + L')L"CT], whereas in CH_2Cl_2 solution the low energy band (408–413 nm) is ascribed mainly to admixture of platina/alkynyl/pq to cyclometalate (pq) charge transfer ^{1}[d(Pt)/C≡C/pq→π*(pq)] ^{1}[(M + L + L')LCT] with contribution to the *N*-donor ligand ^{1}[d(Pt)/C≡C/pq→π*(*N*-donor)]. These assemblies show a stronger luminescence than the starting material (**Pt-1**). The emission properties of the bpe-dimer **4a** in solid state are consistent with a predominantly bpe-centered ^{3}IL ^{3}(ππ*) excited state. However, complexes **1a** and **2a** exhibit emission from an admixture platina/alkynyl to cyclometalated (pq) charge transfer ^{3}[(M + L')LCT], as supported by DFT calculations on **2a**, and in the remaining complexes (**3a**–**5a**) some additional contribution of the central *N*-linker can be invoked. For these complexes, experimental data

(in solid state) and theoretical calculations (in gas phase for **2a**) suggest that the excitation of the molecule seems to introduce a remarkable change in the nature of the HOMO-LUMO/SOMO-SOMO-1, increasing the energy of the π* diimine-based orbitals above the cyclometalated-based orbitals. The emission in solution of the binuclear species (**a**) (predominant in mixtures **Pt-1**:L 1:1) and the mononuclear species; (**b**) (predominant in mixtures Pt-1:L 1:4) is rather similar, suggesting a similar excited state for both types of species, attributed in all complexes to ^{3}[(M + L')LCT].

Acknowledgments

This work was supported by the Spanish MICINN (Projects CTQ2008-06669-C02-02/BQU and CTQ2013-45518-P and a grant for Santiago Ruiz). The authors thank CESGA for computer support.

Author Contributions

Elena Lalinde and M. Teresa Moreno: responsible for research publication (methodology, data analysis and preparation of the manuscript). Santiago Ruiz: experimental work and crystallographic studies. Sergio Sánchez: theoretical calculations.

Conflicts of Interest

The authors declare no conflict of interest.

References

1. Berenguer, J.R.; Lalinde, E.; Moreno, M.T. An overview of the chemistry of homo and heteropolynuclear platinum complexes containing bridging acetylide (μ-C≡CR) ligands. *Coord. Chem. Rev.* **2010**, *254*, 832–857.
2. Lang, H.; George, D.S.A.; Rheinwald, G. Bis(alkynyl) transition metal complexes, $R^1C{\equiv}C$-[M]-$C{\equiv}CR^2$, as organometallic chelating ligands; formation of $\mu,\eta^{1(2)}$-alkynyl-bridged binuclear and oligonuclear complexes. *Coord. Chem. Rev.* **2000**, *206*, 101–197.
3. Lang, H.; Köhler, K.; Blau, S. η^2-Alkyne copper(I) and silver(I) compounds; from polymeric $[M^IR]_n$ to monomeric $[M^IR]$ units (M = Cu, Ag). *Coord. Chem. Rev.* **1995**, *143*, 113–168.
4. Forniés, J.; Lalinde, E. Synthesis, structure and reactivity of homo- and hetero-polynuclear complexes of platinum bearing C≡CR groups as unique bridging ligands. *Dalton Trans.* **1996**, doi:10.1039/DT9960002587.
5. Wong, K.M.C.; Yam, V.W.W. Self-Assembly of Luminescent Alkynylplatinum(II) Terpyridyl Complexes: Modulation of Photophysical Properties through Aggregation Behavior. *Acc. Chem. Res.* **2011**, *44*, 424–434.
6. Yam, V.W.W. Molecular Design of Transition Metal Alkynyl Complexes as Building Blocks for Luminescent Metal-Based Materials: Structural and Photophysical Aspects. *Acc. Chem. Res.* **2002**, *35*, 555–563.
7. Hissler, M.; McGarrah, J.E.; Connick, W.B.; Geiger, D.K.; Cummings, S.D.; Eisenberg, R. Platinum diimine complexes: Towards a molecular photochemical device. *Coord. Chem. Rev.* **2000**, *208*, 115–137.

8. Rossi, E.; Colombo, A.; Dragonetti, C.; Roberto, D.; Ugo, R.; Valore, A.; Falciola, L.; Brulatti, P.; Cocchi, M.; Williams, J.A.G. Novel N^C^N-cyclometallated platinum complexes with acetylide co-ligands as efficient phosphors for OLEDs. *J. Mater. Chem.* **2012**, *22*, 10650–10655.
9. Yam, V.W.W. Luminescent metal alkynyls—From simple molecules to molecular rods and materials. *J. Organomet. Chem.* **2004**, *689*, 1393–1401.
10. Wong, W.Y. Luminescent organometallic poly(aryleneethynylene)s: Functional properties towards implications in molecular optoelectronics. *Dalton Trans.* **2007**, doi:10.1039/B711478H.
11. Chen, Z.N.; Zhao, N.; Fan, Y.; Ni, J. Luminescent groups 10 and 11 heteropolynuclear complexes based on thiolate or alkynyl ligands. *Coord. Chem. Rev.* **2009**, *253*, 1–20.
12. Castellano, F.N.; Pomestchenko, I.E.; Shikhova, E.; Hua, F.; Muro, M.L.; Rajapakse, N. Photophysics in bipyridyl and terpyridyl Platinum(II) acetylides. *Coord. Chem. Rev.* **2006**, *250*, 1819–1828.
13. Wong, K.M.C.; Yam, V.W.W. Luminescence Platinum(II) terpyridyl complexes—From fundamental studies to sensory functions. *Coord. Chem. Rev.* **2007**, *251*, 2477–2488.
14. Mei, J.; Ogawa, K.; Kim, Y.G.; Heston, N.C.; Arenas, D.J.; Nasrollahi, Z.; McCarley, T.D.; Tanner, D.B.; Reynolds, J.R.; Schanze, K.S. Low-Band-Gap Platinum Acetylide Polymers as Active Materials for Organic Solar Cells. *Appl. Mater. Interfaces* **2009**, *1*, 150–161.
15. Colombo, A.; Nisic, F.; Dragonetti, C.; Marinotto, D.; Oliveri, I.P.; Righetto, S.; Lobello, M.G.; De Angelis, F. Unexpectedly high second-order nonlinear optical properties of simple Ru and Pt alkynyl complexes as an analytical springboard for NLO-active polymer films. *Chem. Commun.* **2014**, *50*, 7986–7989.
16. Rossi, E.; Colombo, A.; Dragonetti, C.; Righetto, S.; Roberto, D.; Ugo, R.; Valore, A.; Williams, J.A.G.; Lobello, M.G.; De Angelis, F. Tuning the Dipolar Second-Order Nonlinear Optical Properties of Cyclometalated Platinum(II) Complexes with Tridentate N^C^N Binding Ligands. *Chem. Eur. J.* **2013**, *19*, 9875–9883.
17. Green, K.A.; Cifuentes, M.P.; Samoc, M.; Humphrey, M.G. Metal alkynyl complexes as switchable NLO systems. *Coord. Chem. Rev.* **2011**, *255*, 2530–2541.
18. Berenguer, J.R.; Forniés, J.; Lalinde, E.; Martín, A.; Serrano, B. Preparation and characterisation of neutral double- and mono-alkynyl bridged diplatinum complexes. *Dalton Trans.* **2001**, doi:10.1039/B104783N.
19. Ara, I.; Falvello, L.R.; Fernández, S.; Forniés, J.; Lalinde, E.; Martín, A.; Moreno, M.T. Synthesis and Reactivity of σ-Alkynyl/*P*-Bonded Phosphinoalkyne Platinum Complexes toward *cis*-[M(C_6F_5)$_2$(thf)$_2$] (M = Pt, Pd). *Organometallics* **1997**, *16*, 5923–5937.
20. García, A.; Lalinde, E.; Moreno, M.T. Ethynyltolan Platinum Complexes with (Arylalkynyl)phosphane Ligands. *Eur. J. Inorg. Chem.* **2007**, *2007*, 3553–3560.
21. Forniés, J.; Gómez-Saso, M.A.; Lalinde, E.; Martínez, F.; Moreno, M.T. Preparation of Doubly Acetylide-Bridged Binuclear Platinum-Platinum and Platinum-Palladium Complexes. Structures of [{(dppe)Pt(C≡CPh)$_2$}Pt(C_6F_5)$_2$] and (PMePh$_3$)$_2$[(C_6F_5)$_2$Pt(μ-C≡CPh)$_2$Pt(C_6F_5)$_2$]. *Organometallics* **1992**, *11*, 2873–2883.
22. Falvello, L.R.; Forniés, J.; Gómez, J.; Lalinde, E.; Martín, A.; Martínez, F.; Moreno, M.T. Some Platinum(II) complexes containing bis(diphenylphosphino)acetylene $PPh_2C{\equiv}CPPh_2$: Synthesis, characterisation and crystal structures. *Dalton Trans.* **2001**, doi:10.1039/B101558N.

23. Berenguer, J.R.; Forniés, J.; Martínez, F.; Cubero, J.C.; Lalinde, E.; Moreno, M.T.; Welch, A.J. Synthesis and reactivity of bimetallic acetylide-bridged Pt-Pt complexes. Crystal and molecular structure of [(PPh$_3$)(C$_6$F$_5$)Pt(μ-C≡CPh)$_2$Pt(C$_6$F$_5$)(PPh$_3$)]. *Polyhedron* **1993**, *12*, 1797–1804.
24. Falvello, L.R.; Forniés, J.; Martín, A.; Gómez, J.; Lalinde, E.; Moreno, M.T.; Sacristán, J. Synthesis of Heterobridged (μ-C≡CR)(μ-X) (X = PPh$_2$, PPh$_2$O) Platinum−Rhodium or Platinum−Iridium Dimers. *Inorg. Chem.* **1999**, *38*, 3116–3125.
25. Aullón, G.; Álvarez, S. Molecular Structure and Isomerization in Square-Planar Edge-Sharing Dinuclear Complexes with Alkynyl Bridges. *Organometallics* **2002**, *21*, 2627–2634.
26. Hoogervorst, W.J.; Elsevier, C.J.; Lutz, M.; Spek, A.L. New *cis*- and *trans*-ArylPlatinum(II) Acetylide Compounds Containing a Bis(imino)aryl [NCN] Ligand. *Organometallics* **2001**, *20*, 4437–4440.
27. Casas, J.M.; Forniés, J.; Fuertes, S.; Martín, A.; Sicilia, V. New Mono- and Polynuclear Alkynyl Complexes Containing Phenylacetylide as Terminal or Bridging Ligand. X-ray Structures of the Compounds NBu$_4$[Pt(CH$_2$C$_6$H$_4$P(*o*-tolyl)$_2$-κ*C*,*P*)(C≡CPh)$_2$], [Pt(CH$_2$C$_6$H$_4$P(*o*-tolyl)$_2$-κ*C*,*P*)(C≡CPh)(CO)], [{Pt(CH$_2$C$_6$H$_4$P(*o*-tolyl)$_2$-κ*C*,*P*)(C≡CPh)}$_2$], and [{Pt(CH$_2$C$_6$H$_4$P(*o*-tolyl)$_2$-κ*C*,*P*)(C≡CPh)$_2$Cu}$_2$]. *Organometallics* **2007**, *26*, 1674–1685.
28. Forniés, J.; Lalinde, E.; Martín, A.; Moreno, M.T. Di- and tri-nuclear platinum complexes with double acetylide bridges. Molecular structure of [NBu$_4$]$_2$[Pt$_3$(C$_6$F$_5$)$_4$(μ-C≡CPh)$_4$] 4thf (thf = tetrahydrofuran). *Dalton Trans.* **1994**, doi:10.1039/DT9940000135.
29. Berenguer, J.R.; Forniés, J.; Lalinde, E.; Martínez, F. Unusual stabilization of cationic M(η^3-allyl)$^{+n}$ (M = Pt, Pd) units by a dianionic *cis*-{Pt(C$_6$F$_5$)$_2$(C≡CSiMe$_3$)$_2$}$^{2-}$ fragment. *J. Organomet. Chem.* **1994**, *470*, C15–C18.
30. Fujita, M.; Yazaki, J.; Ogura, K. Preparation of a macrocyclic polynuclear complex, [(en)Pd(4,4'-bpy)]$_4$(NO$_3$)$_8$ (en = ethylenediamine, bpy = bipyridine), which recognizes an organic molecule in aqueous media. *J. Am. Chem. Soc.* **1990**, *112*, 5645–5647.
31. Zangrando, E.; Casanova, M.; Alessio, E. Trinuclear Metallacycles: Metallatriangles and Much More. *Chem. Rev.* **2008**, *108*, 4979–5013.
32. Fujita, M. Metal-directed self-assembly of two- and three-dimensional synthetic receptors. *Chem. Soc. Rev.* **1998**, *27*, 417–425.
33. Caulder, D.L.; Raymond, K.N. Supermolecules by Design. *Acc. Chem. Res.* **1999**, *32*, 975–982.
34. Leininger, S.; Olenyuk, B.; Stang, P.J. Self-Assembly of Discrete Cyclic Nanostructures Mediated by Transition Metals. *Chem. Rev.* **2000**, *100*, 853–908.
35. Navarro, J.A.R.; Lippert, B. Simple 1:1 and 1:2 complexes of metal ions with heterocycles as building blocks for discrete molecular as well as polymeric assemblies. *Coord. Chem. Rev.* **2001**, *222*, 219–250.
36. Fujita, M.; Tominaga, M.; Hori, A.; Therrien, B. Coordination Assemblies from a Pd(II)-Cornered Square Complex. *Acc. Chem. Res.* **2005**, *38*, 369–378.
37. Nitschke, J.R. Construction, Substitution, and Sorting of Metallo-organic Structures via Subcomponent Self-Assembly. *Acc. Chem. Res.* **2006**, *40*, 103–112.
38. Schmidt, A.; Casini, A.; Kühn, F.E. Self-assembled M$_2$L$_4$ coordination cages: Synthesis and potential applications. *Coord. Chem. Rev.* **2014**, *275*, 19–36.

39. Amouri, H.; Desmarets, C.; Moussa, J. Confined Nanospaces in Metallocages: Guest Molecules, Weakly Encapsulated Anions, and Catalyst Sequestration. *Chem. Rev.* **2012**, *112*, 2015–2041.
40. Desmarets, C.; Ducarre, T.; Rager, M.N.; Gontard, G.; Amouri, H. Self-Assembled M_2L_4 Nanocapsules: Synthesis, Structure and Host-Guest Recognition Toward Square Planar Metal Complexes. *Materials* **2014**, *7*, 287–301.
41. Desmarets, C.; Gontard, G.; Cooksy, A.L.; Rager, M.N.; Amouri, H. Encapsulation of a Metal Complex within a Self-Assembled Nanocage: Synergy Effects, Molecular Structures, and Density Functional Theory Calculations. *Inorg. Chem.* **2014**, *53*, 4287–4294.
42. Kaiser, A.; Bäuerie, P. Macrocycles and complex three-dimensional structures comprising Pt(II) building blocks. *Top. Curr. Chem.* **2005**, *249*, 127–201.
43. Pollock, J.B.; Schneider, G.L.; Cook, T.R.; Davies, A.S.; Stang, P.J. Tunable Visible Light Emission of Self-Assembled Rhomboidal Metallacycles. *J. Am. Chem. Soc.* **2013**, *135*, 13676–13679.
44. Pollock, J.B.; Cook, T.R.; Stang, P.J. Photophysical and Computational Investigations of Bis(phosphine) OrganoPlatinum(II) Metallacycles. *J. Am. Chem. Soc.* **2012**, *134*, 10607–10620.
45. Chen, J.S.; Zhao, G.J.; Cook, T.R.; Han, K.L.; Stang, P.J. Photophysical Properties of Self-Assembled Multinuclear Platinum Metallacycles with Different Conformational Geometries. *J. Am. Chem. Soc.* **2013**, *135*, 6694–6702.
46. Chen, J.S.; Zhao, G.J.; Cook, T.R.; Sun, X.F.; Yang, S.Q.; Zhang, M.X.; Han, K.L.; Stang, P.J. Experimental and Theoretical Study on the Photophysical Properties of 90° and 60° Bimetallic Platinum Complexes. *J. Phys. Chem. A* **2012**, *116*, 9911–9918.
47. Zhao, G.J.; Yu, F.; Zhang, M.X.; Northrop, B.H.; Yang, H.; Han, K.L.; Stang, P.J. Substituent Effects on the Intramolecular Charge Transfer and Fluorescence of Bimetallic Platinum Complexes. *J. Phys. Chem. A* **2011**, *115*, 6390–6393.
48. Allendorf, M.D.; Bauer, C.A.; Bhakta, R.K.; Houk, R.J.T. Luminescent metal-organic frameworks. *Chem. Soc. Rev.* **2009**, *38*, 1330–1352.
49. Jude, H.; Krause, B.J.A.; Connick, W.B. Luminescent Platinum(II) Dimers with a Cyclometallating Aryldiamine Ligand. *Inorg. Chem.* **2005**, *44*, 1211–1220.
50. Jude, H.; Krause, B.J.A.; Connick, W.B. Tuning the Electronic Structures of Platinum(II) Complexes with a Cyclometalating Aryldiamine Ligand. *Inorg. Chem.* **2004**, *43*, 725–733.
51. Shi, L.L.; Liao, Y.; Yang, G.C.; Su, Z.M.; Zhao, S.S. Effect of π-Conjugated Length of Bridging Ligand on the Optoelectronic Properties of Platinum(II) Dimers. *Inorg. Chem.* **2008**, *47*, 2347–2355.
52. Jude, H.; Krause Bauer, J.A.; Connick, W.B. Synthesis, Structures, and Emissive Properties of Platinum(II) Complexes with a Cyclometallating Aryldiamine Ligand. *Inorg. Chem.* **2002**, *41*, 2275–2281.
53. Fuertes, S.; Woodall, C.H.; Raithby, P.R.; Sicilia, V. Heteropolynuclear Pt(II)–M(I) Clusters with a C^N^C Biscyclometalated Ligand. *Organometallics* **2012**, *31*, 4228–4240.
54. Zhao, F.; Xu, X.; Khoo, S.B.; Hor, T.S.A. Structure-Dependent Electrochemical Behavior of Thienylplatinum(II) Complexes of *N*,*N*-Heterocycles. *Eur. J. Inorg. Chem.* **2004**, *1*, 69–77.

55. Rao, Y.L.; Wang, S. Impact of Constitutional Isomers of (BMes2)phenylpyridine on Structure, Stability, Phosphorescence, and Lewis Acidity of Mononuclear and Dinuclear Pt(II) Complexes. *Inorg. Chem.* **2009**, *48*, 7698–7713.
56. Meijer, M.D.; de Wolf, E.; Lutz, M.; Spek, A.L.; van Klink, G.P.M.; van Koten, G. *C*,*N*-2-[(Dimethylamino)methyl]phenylplatinum Complexes Functionalized with C_{60} as Macromolecular Building Blocks. *Organometallics* **2001**, *20*, 4198–4206.
57. Lalinde, E.; Moreno, M.T.; Ruiz, S.; Sánchez, S. Synthesis, Structural and Photophysical Studies of Phenylquinoline and Phenylquinolinyl Alkynyl Based Pt(II) Complexes. *Organometallics* **2014**, *33*, 3078–3090.
58. Berenguer, J.R.; Díez, A.; Lalinde, E.; Moreno, M.T.; Ruiz, S.; Sánchez, S. Luminescent Cycloplatinated Complexes Containing Poly(pyrazolyl)-borate and -methane Ligands. *Organometallics* **2011**, *30*, 5776–5792.
59. Dattelbaum, D.M.; Itokazu, M.K.; Murakami, I.N.Y.; Meyer, T.J. Mechanism of Metal-to-Ligand Charge Transfer Sensitization of Olefin *trans*-to-*cis* Isomerization in the *fac*-$[Re^{I}(phen)(CO)_3(1,2\text{-bpe})]^+$ Cation. *J. Phys. Chem. A* **2003**, *107*, 4092–4095.
60. Schanze, K.S.; Lucia, L.A.; Cooper, M.; Walters, K.A.; Ji, H.F.; Sabina, O. Intramolecular Energy Transfer to *trans*-Stilbene. *J. Phys. Chem. A* **1998**, *102*, 5577–5584.
61. Saltiel, J.; Marchand, G.R.; Kirkor-Kaminska, E.; Smothers, W.K.; Mueller, W.B.; Charlton, J.L. Nonvertical triplet excitation transfer to *cis*- and *trans*-stilbene. *J. Am. Chem. Soc.* **1984**, *106*, 3144–3151.
62. Coe, B.J.; Harries, J.L.; Harris, J.A.; Brunschwig, B.S.; Coles, S.J.; Light, M.E.; Hursthouse, M.B. Syntheses, spectroscopic and molecular quadratic nonlinear optical properties of dipolar ruthenium(II) complexes of the ligand 1,2-phenylenebis(dimethylarsine). *Dalton Trans.* **2004**, doi:10.1039/B409432H.
63. Amoroso, A.J.; Cargill T.A.M.W.; Maher, J.P.; McCleverty, J.A.; Ward, M.D. Di-, Tri-, and Tetranucleating Pyridyl Ligands Which Facilitate Multicenter Magnetic Exchange between Paramagnetic Molybdenum Centers. *Inorg. Chem.* **1995**, *34*, 4828–4835.
64. Otwinowsky, Z.; Minor, W. *Methods Enzymol.*; Academic Press: New York, NY, USA, 1997; Volume 276A, pp. 307–326.
65. Burla, M.C.; Caliandro, R.; Camalli, M.; Carrozzini, B.; Cascarano, G.L.; De Caro, L.; Giacovazzo, C.; Polidori, G.; Spagna, R. SIR2004: An improved tool for crystal structure determination and refinement. *J. App. Crystallogr.* **2005**, *38*, 381–388.
66. *SHELX-97*; University of Göttingen: Göttingen, Germany, 1997.
67. Cambridge Crystallographic Data Centre. Available online: http://www.ccdc.cam.ac.uk/data_request/cif (accessed on 11 October 2014).
68. *Gaussian 03*; Gaussian, Inc.: Wallingford, CT, USA, 2004.
69. Becke, A.D. Density-functional exchange-energy approximation with correct asymptotic behavior. *Phys. Rev. A* **1988**, *38*, 3098–3100.
70. Lee, C.; Yang, W.; Parr, R.G. Development of the Colle-Salvetti correlation-energy formula into a functional of the electron density. *Phys. Rev. B* **1988**, *37*, 785–789.
71. Becke, A.D. Density-functional thermochemistry. III. The role of exact exchange. *J. Chem. Phys.* **1993**, *98*, 5648–5652.

72. Wadt, W.R.; Hay, P.J. Ab initio effective core potentials for molecular calculations. Potentials for main group elements Na to Bi. *J. Chem. Phys.* **1985**, *82*, 284–298.
73. Barone, V.; Cossi, M. Quantum Calculation of Molecular Energies and Energy Gradients in Solution by a Conductor Solvent Model. *J. Phys. Chem. A* **1998**, *102*, 1995–2001.
74. Cossi, M.; Rega, N.; Scalmani, G.; Barone, V. Energies, structures, and electronic properties of molecules in solution with the C-PCM solvation model. *J. Comput. Chem.* **2003**, *24*, 669–681.